



TRANSIT TIMING OBSERVATIONS FROM *KEPLER*. IX. CATALOG OF THE FULL LONG-CADENCE DATA SET

TOMER HOLCZER¹, TSEVI MAZEH¹, GIL NACHMANI¹, DANIEL JONTOF-HUTTER², ERIC B. FORD^{2,3}, DANIEL FABRYCKY⁴, DARIN RAGOZZINE⁵, MACKENZIE KANE⁵, AND JASON H. STEFFEN⁶

¹ School of Physics and Astronomy, Raymond and Beverly Sackler Faculty of Exact Sciences, Tel Aviv University, Tel Aviv 69978, Israel; tomer.holczer@gmail.com

² Department of Astronomy and Astrophysics, The Pennsylvania State University, 525 Davey Laboratory, University Park, PA 16802, USA

³ Center for Exoplanets and Habitable Worlds, 525 Davey Laboratory, The Pennsylvania State University, University Park, PA, 16802, USA

⁴ Department of Astronomy and Astrophysics, University of Chicago, 5640 South Ellis Avenue, Chicago, IL 60637, USA

⁵ Department of Physics and Space Sciences, Florida Institute of Technology, 150 West University Boulevard, Melbourne, FL 32901, USA

⁶ CIERA, Northwestern University, 2145 Sheridan Road, Evanston, IL 60208, USA; jsteffen@fnal.gov

Received 2015 July 20; revised 2016 April 7; accepted 2016 April 7; published 2016 July 22

ABSTRACT

We present a new transit timing catalog of 2599 *Kepler* Objects of Interest (KOIs), using the PDC-MAP long-cadence light curves that include the full 17 quarters of the mission (ftp://wise-ftp.tau.ac.il/pub/tautv/TTV_ver_112). The goal is to produce an easy-to-use catalog that can stimulate further analyses of interesting systems. For 779 KOIs with high enough S/N, we derived the timing, duration, and depth of 69,914 transits. For 1820 KOIs with lower SNR, we derived only the timing of 225,273 transits. After removal of outlier timings, we derived various statistics for each KOI that were used to indicate significant variations. Including systems found by previous works, we have detected 260 KOIs that showed significant TTVs with long-term variations (>100 days), and another 14 KOIs with periodic modulations shorter than 100 days and small amplitudes. For five of those, the periodicity is probably due to the crossing of rotating stellar spots by the transiting planets.

Key words: planets and satellites: detection – techniques: miscellaneous – techniques: photometric

Supporting material: machine-readable tables

1. INTRODUCTION

More than four years of almost uninterrupted performance of the *Kepler* mission produced about 190,000 light curves with high precision, leading to the discovery of more than 8000 planet candidates (=KOIs)⁷ that show periodic shallow transits caused by small eclipsing objects. Many of the KOIs display shifts of the transit timings (O-Cs) relative to a strict periodicity, which is expected if the transiting planets were to move on a Keplerian orbit. These O-Cs, sometimes called transit time variations (=TTVs), can indicate a dynamical interaction with additional objects in the system, as was predicted by the seminal works of Holman & Murray (2005) and Agol et al. (2005).

Indeed, TTVs turned out to be a crucial tool in the study of systems with known multiple transiting planets (e.g., Holman et al. 2010; Cochran et al. 2011; Lissauer et al. 2011a; Fabrycky et al. 2012; Ford et al. 2012a; Steffen et al. 2012b; Weiss et al. 2013; Xie 2013, 2014; Yang et al. 2013; Jontof-Hutter et al. 2014; Masuda 2014; Ofir et al. 2014; Agol & Deck 2015). Furthermore, observed TTVs may indicate extra *non-transiting* planets through their dynamical interaction with the transiting ones (Ballard et al. 2011; Nesvorný et al. 2012, 2013, 2014; Dawson et al. 2014).

Therefore, it can be useful to perform a systematic TTV search of all KOIs, as was done by Ford et al. (2011, 2012b) and Steffen et al. (2012a) at the early stages of the mission. As *Kepler* released more data, additional systematic analyses were performed, using the longer light curves that became available (see Mazeh et al. 2013; Szabó et al. 2013). Based on the first 12 *Kepler* quarters, a global analysis of all KOIs, including the

timing of the transits, was published recently by Rowe et al. (2015). In a follow-up publication Rowe & Thompson (2015) listed 258 KOIs with significant TTVs, based on the first 16 quarters.

The *Kepler* mission in its original mode of operation has been terminated after 17 quarters, and is now on its *K2* mode (Howell et al. 2014), and we do not expect any additional *Kepler* TTVs for the KOIs identified during the original mission. Thus, here we analyze the whole data set of the mission and derive a complete catalog of the transit timings. Following the approach of Mazeh et al. (2013), we present here an analysis of 2599 KOIs, based on all 17 quarters of the *Kepler* data. The goal is to produce an easy-to-use catalog that can stimulate further analysis of interesting systems and a statistical analysis of the *Kepler* KOIs with significant long-term TTVs.

After presenting the details of our pipeline and the catalog itself in Section 2, we derive in Section 3 a few statistical characteristics of the timing series of each KOI which can identify significant variations. Sections 4 and 5 list and display 274 systems with significant TTVs, and Section 8 summarizes and discusses briefly the potential of the catalog.

2. ANALYSIS OF THE TRANSIT LIGHT CURVES

The analysis presented here is based on the list of 4690 KOIs in the NASA Exoplanet Archive,⁸ as of 2013 November 23rd, ignoring KOIs listed as false positives. We did not analyze 2091 KOIs, for which at least one of the following is true:

⁷ <http://exoplanetarchive.ipac.caltech.edu/>

⁸ <http://exoplanetarchive.ipac.caltech.edu/>

Table 1
Additional False Positive KOIs

| KOI |
|---------|---------|---------|---------|---------|---------|---------|---------|
| 225.01 | 302.01 | 823.01 | 977.01 | 1351.01 | 1452.01 | 1701.01 | 1771.01 |
| 2014.01 | 3175.01 | 3244.01 | 3272.01 | 3290.01 | 3331.01 | 3467.01 | 3565.01 |
| 3606.01 | 3715.01 | 4135.01 | 4294.01 | 4351.01 | 4925.01 | 4936.01 | 4937.01 |
| 4944.01 | 4947.01 | 4951.01 | 4953.01 | 4968.01 | 4970.01 | 5011.01 | 5015.01 |
| 5025.01 | 5061.01 | 5068.01 | 5076.01 | 5087.01 | 5090.01 | 5111.01 | 5112.01 |
| 5145.01 | 5152.01 | 5171.01 | 5172.01 | 5173.01 | 5218.01 | 5233.01 | 5255.01 |
| 5293.01 | 5295.01 | 5305.01 | 5306.01 | 5353.01 | 5354.01 | 5369.01 | 5392.01 |
| 5448.01 | 5460.01 | 5463.01 | 5542.01 | 5564.01 | 5569.01 | 5587.01 | 5683.01 |
| 5714.01 | 5733.01 | 5774.01 | 5780.01 | 5797.01 | 5828.01 | 5894.01 | 5906.01 |
| 5976.01 | | | | | | | |

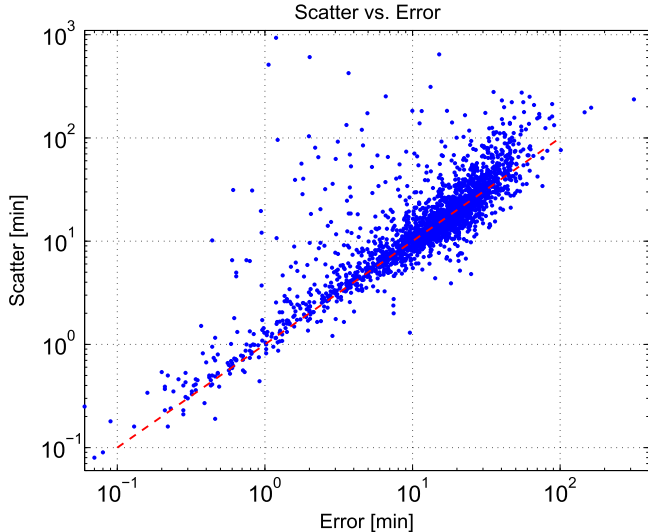


Figure 1. Scatter of the derived O-C timings as a function of their typical uncertainty for 2339 KOIs with at least 7 transit timings. The dashed line is the locus of points for which the scatter is equal to the typical error.

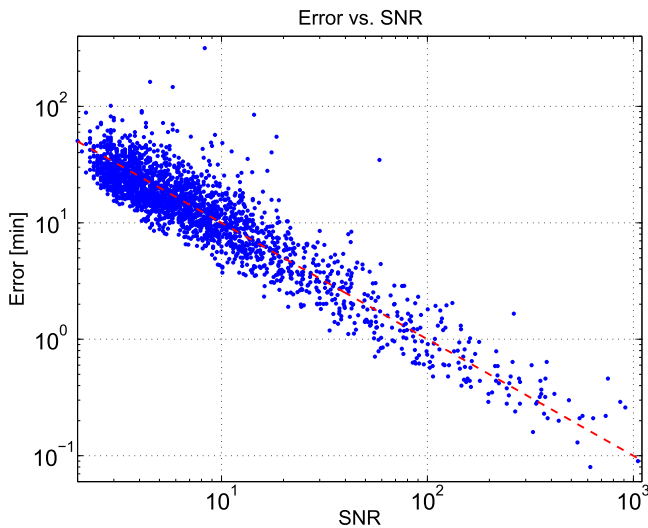


Figure 2. Typical transit timing uncertainty as a function of the typical SNR of a single transit for each KOI. The dashed red line represents $\bar{\sigma}_{\text{TT}} = (100 \text{ minutes})/\text{SNR}$.

1. The folded light curve did not display a significant transit, either because the folded transit's SNR (defined as the transit depth of the model, divided by the median uncertainty of the individual points of the light curve,

and multiplied by the square root of the number of measurements at the folded transit, including its ingress and egress) was smaller than 7.1, similar to the criterion used by Batalha et al. (2013), or where the p -value of the transit model exceeded 10^{-4} , using an \mathcal{F} -test relative to the no-transit assumption.

2. The transit depth was larger than 10%; those KOIs were ignored in order to disregard eclipsing binaries in our analysis, with the price of leaving out some “legitimate” transits such as large planets around M-stars.
3. The orbital period >300 days; those KOIs were ignored due to too few transits for a significant TTV analysis.
4. KOIs identified as EBs, either listed in the Villanova eclipsing binary catalog,⁹ as of 2014 July, or by McQuillan et al. (2013).
5. KOIs identified by this study as false alarm, listed in Table 1, with some evidence for stellar binarity or pulsation.

Following these cuts we were left with 2599 KOIs. We started by folding the PDC-MAP *Kepler* long-cadence¹⁰ data, with the BJD_{TDB} timings, using the ephemeris of NASA Exoplanet Archive in order to obtain a good template for the transit light curve (see below for details). We used the best-fit transit model to measure the timing of each individual transit (=TT) and derived its O-C—the difference between the TT and the expected time, based on a linear ephemeris. As in Mazeh et al. (2013), for KOIs with high enough SNR (see below), the TT derivation was performed while allowing the duration and depth of each transit to vary.

2.1. Detrending

The first step of our analysis was finding the continuum around each transit, ignoring the points in or near the transit itself, up to 0.7 transit durations around the expected timing of the transit center. Looking at a more extended region, up to two durations around the expected transit center, we fitted six different polynomials of degrees one to six to that region. The best fit was chosen as the one with the highest degree for which the p -value of all the \mathcal{F} -tests with regard to polynomial fits of lower degrees was lower than 10^{-3} . Finally, we added this polynomial back to the data during transit and divided the light curve in the entire region by that polynomial.

⁹ <http://keplerebs.villanova.edu/>

¹⁰ <ftp://archive.stsci.edu/pub/kepler/lightcurves/tarfiles>

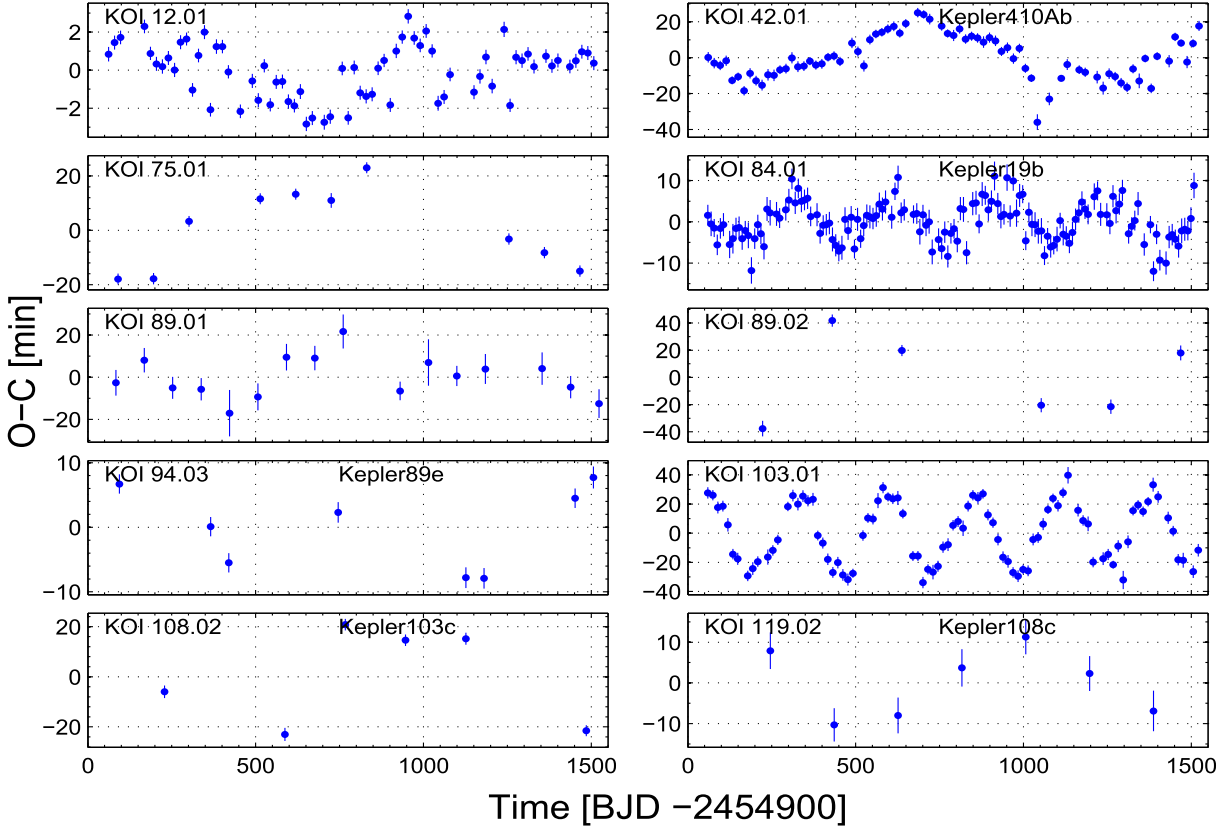


Figure 3. KOIs with significant long-term TTVs.

Table 2
KOI Transits: Linear Ephemerides, Duration, and Depth

KOI	T_0^a (days)	Period ^b (days)	Duration ^c (hr)	Depth ^d (ppm)	SNR ^e	Scatter ^f Ratio
1.01	55.763337 ± 0.000006	2.47061338 ± 0.00000001	1.8638	14210	618.0	1.66 ...
2.01	54.358470 ± 0.000014	2.20473540 ± 0.00000002	4.0398	6694	368.6	1.14 ...
3.01	57.813556 ± 0.000033	4.88780267 ± 0.00000004	2.5819	4361	266.8	2.17 ...
5.01	56.414171 ± 0.000158	4.78032873 ± 0.00000018	2.1266	980	34.9	0.94 ...
7.01	56.612028 ± 0.000272	3.21366739 ± 0.00000032	4.2575	736	24.6	1.00 ...
10.01	54.119425 ± 0.000045	3.52249865 ± 0.00000005	3.3119	9370	127.3	1.17 ...
12.01	61.739669 ± 0.000246	17.85523009 ± 0.00000028	7.3728	9228	357.1	2.26 ...
13.01	53.565659 ± 0.000010	1.76358757 ± 0.00000001	3.3504	4602	535.1	1.30 ...
17.01	54.486657 ± 0.000028	3.23469918 ± 0.00000003	3.7108	10811	248.6	1.19 ...
18.01	55.901581 ± 0.000042	3.54846550 ± 0.00000005	4.6623	7454	161.6	1.16 ...

Notes.^a T_0 (BJD-2454900).^b Orbital period (days).^c Transit duration (hr).^d Transit depth (ppm).^e Median single-transit SNR.^f Scatter inside the transit to scatter outside the transit ratio.

(This table is available in its entirety in machine-readable form.)

Table 3
TTV, Duration (TDV), and Depth (TPV) Changes of the Transits

KOI	n^a	t_n^b (days)	TTV_n^c (minutes)	σ_n^d (minutes)	TDV_n^e	σ_n^f	TPV_n^g	σ_n^h	Outlier ⁱ Flag	Overlap ^j Flag
1.01	0	55.7633	-0.050	0.085	0.001	0.003	-0.006	0.003	0	0
1.01	1	58.2340	0.077	0.086	-0.002	0.003	-0.008	0.003	0	0
1.01	2	60.7046	-0.037	0.086	0.001	0.002	-0.011	0.003	0	0
1.01	4	65.6458	-0.271	0.086	0.001	0.002	-0.003	0.003	4	0
1.01	5	68.1164	-0.003	0.085	-0.001	0.002	-0.002	0.003	0	0
1.01	6	70.5870	0.061	0.085	-0.003	0.003	-0.002	0.003	0	0
1.01	7	73.0576	0.175	0.087	0.019	0.003	-0.030	0.003	0	0
1.01	8	75.5282	0.186	0.085	0.004	0.003	-0.003	0.003	0	0
1.01	9	77.9989	0.047	0.082	-0.007	0.003	0.005	0.003	0	0
1.01	10	80.4695	-0.082	0.085	0.005	0.003	-0.012	0.003	0	0

Notes.^a Transit number.^b Expected transit time of the linear ephemeris (BJD-2454900).^c O-C time difference.^d O-C uncertainty.^e Fractional duration variation: (duration of transit—average)/average.^f TDV uncertainty.^g Fractional depth variation.^h TPV uncertainty.ⁱ Outlier flag. Sum of: 0 = not an outlier, 1 = no-variation p -value > 0.025 , 2 = local TTV, 4 = global TTV, 8 = global TDV, 16 = global TPV, 32 = TTV, TDV or TPV uncertainty outlier (see Section 2.4).^j Overlapping flag: 0 = no overlapping, 1 = another relatively large interfering transit (> 0.25 the “area” of the transit) too close (expected time difference < 2 transit durations +1 interfering transit duration).

(This table is available in its entirety in machine-readable form.)

Table 4
Statistical Parameters of the O-Cs Series

KOI	$\bar{\sigma}_{\text{TT}}^a$ (minutes)	$s_{\text{O-C}}^b$ (minutes)	$p\text{-s}/\sigma^c$ (log)	PS Period ^d (days)	PS Peak ^e (log)	$p\text{-PS}^f$ (log)	\mathcal{A}^g (log)	$p\text{-}\mathcal{A}^h$ (log)	Pol. Deg. ⁱ	$p\text{-}\mathcal{F}^j$ (log)
1.01	0.08	0.09	0.0	17.40	-9.54	0.0	0.188	-0.9	1	-0.2
2.01	0.23	0.24	0.0	4.43	-8.75	-0.6	0.036	-0.3	1	-1.3
3.01	0.24	0.35	-0.2	13.94	-8.11	-0.1	0.220	-0.6	2	-2.7
5.01	1.65	1.73	0.0	52.05	-6.81	-0.2	-0.064	-0.5	1	-0.1
7.01	3.54	3.28	0.0	8.31	-6.19	-0.2	0.038	-1.1	1	-0.3
10.01	0.60	0.59	0.0	26.03	-7.90	0.0	-0.278	-0.4	1	-0.2
12.01	0.37	1.51	< -16.0	1176.37	-6.24	-3.3	3.234	< -4.0	2	-3.9
13.01	0.13	0.16	0.0	5.72	-8.83	-1.1	-0.104	-2.7	1	-1.1
17.01	0.33	0.40	0.0	10.89	-8.10	-0.6	0.046	-0.6	1	-0.2
18.01	0.57	0.56	0.0	23.72	-7.83	-0.2	-0.104	-0.5	1	-0.1

Notes.^a O-C uncertainty median.^b O-C scatter (1.483 times the MAD).^c The p -value of the scatter divided by the uncertainty (see the text).^d The period with the highest peak in the power spectrum.^e The amplitude of the highest peak in the power spectrum, in days squared.^f The logarithm of the p -value of the \mathcal{F} -test for the highest PS peak found.^g Alarm score (see the text).^h The logarithm of the p -value of the alarm found.ⁱ The degree of the best fitting polynomial.^j The logarithm of the p -value of the \mathcal{F} -test for the best polynomial fit.

(This table is available in its entirety in machine-readable form.)

2.2. The Transit Model

After detrending, all transits were folded with the transit period and fit with a transit model. As in Mazeh et al. (2013), we used three different model templates to fit the folded data: a Mandel & Agol (2002), a Legendre polynomial and a Fermi

function template model. We computed these three models for each KOI, and chose the model with the lowest χ^2 value as the transit template. The Mandel–Agol model was averaged to fit the long exposures of the mission, and used a quadratic limb-darkening law of two free parameters. Because we were

Table 5
KOIs with Significant Long-term TTV

KOI	Period ^a (days)	Model ^b	Period ^c (days)	σ_p^d (days)	Ampe (minutes)	σ_A^e (minutes)	Res ^g (minutes)	N ^h	Multiplicity ⁱ	References
12.01	17.86	Cos	1246	60	1.152	0.081	1.2	69	1	
42.01	17.83	Cos	960.6	9.2	15.59	0.49	4.1	75	1	(3) Kepler410Ab
75.01	105.88	Pol	~20	...	4	10	1	
84.01	9.29	Cos	313.5	2.1	5.03	0.34	2.9	142	1	(4) Kepler19b
89.01	84.69	Cos	550	23	8.9	2.6	5.2	16	2	
89.02	207.59	Cos	1440	110	55	13	12	6	2	
94.03	54.32	Cos	682	16	8.7	1.3	0.83	8	4	(5) Kepler89e
103.01	14.91	Cos	262.48	0.63	26.63	0.63	5.6	90	1	(1),(2)
108.02	179.61	Pol	~15	...	4	6	2	(6) Kepler103c
119.02	190.32	Cos	881	56	10.7	2.7	1.1	7	2	(7) Kepler108c
137.01	7.64	Cos	269.4	1.4	4.3	0.23	2.7	157	3	(1), (8) Kepler18c
137.02	14.86	Cos	267.6	1.4	4.49	0.27	1.5	71	3	(1), (2), (8) Kepler18d
139.01	224.83	Cos	2213	79	211	22	13	7	2	(7) Kepler111c
142.01	10.95	Cos	627.52	0.08	649.77	0.62	59	119	1	(1), (2), (9) Kepler88b
		Cos	331.75	0.12	105.32	0.45	59			
152.01	52.09	Cos	614	13	8.6	1.3	5.8	26	4	(7) Kepler79d
152.02	27.40	Cos	963	47	14.3	2.5	9.8	40	4	(10) Kepler79c
152.03	13.48	Cos	849	35	9.4	1.4	9.4	85	4	(10) Kepler79b
152.04	81.06	Cos	738	38	34	9.1	10	14	4	(7) Kepler79e
157.01	13.02	Cos	229.3	3.2	6.9	1.6	5.9	69	6	(11) Kepler11c
157.03	32.00	Cos	182.7	2	6.4	1.9	6.3	33	6	(11) Kepler11e
		Cos	138.7	1.2	5.2	1.2	6.3			
157.04	46.69	Cos	558	11	26.3	4.4	3.4	18	6	(2),(11) Kepler11f
165.01	13.22	Cos	522	18	4	1.2	5.8	92	1	
166.01	12.49	Cos	288.1	7.5	3.9	1.1	5.1	102	1	
168.01	10.74	Cos	456.8	5.8	22.5	2.8	10	88	3	(2),(12) Kepler23c
168.03	7.11	Cos	451	12	46	11	30	72	3	(12) Kepler23b
202.01	1.72	Pol	~0.3	...	0.61	728	1	(13) Kepler412b
226.01	8.31	Cos	606	18	9.2	1.7	10	144	1	
227.01	17.67	Cos	1546.6	3	924	2.8	20	59	1	(1),(2)
244.01	12.72	Cos	329.1	3.9	1.48	0.16	1.2	93	2	(1),(14) Kepler25c
244.02	6.24	Cos	326.3	3.1	3.82	0.32	3.2	195	2	(1), (2), (14) Kepler25b
248.01	7.20	Cos	368	3.2	11.5	0.92	7.6	122	4	(1), (2), (15) Kepler49b
248.02	10.91	Cos	369.6	3.5	20.9	1.7	6.9	79	4	(1),(15) Kepler49c
250.01	12.28	Cos	751	12	9.58	0.65	6.9	98	4	(14) Kepler26b
250.02	17.25	Cos	734	18	9.9	1	7.9	68	4	(1),(14) Kepler26c
262.01	7.81	Cos	1060	24	34.8	2.1	16	117	2	(15) Kepler50b
262.02	9.38	Cos	664	11	15.4	1.4	12	114	2	(15) Kepler50c
271.02	29.39	Cos	1076	65	9.8	2.1	8.9	42	3	(7) Kepler127c
274.01	15.09	Cos	955	30	66.3	7.7	43	59	2	(10) Kepler128b
274.02	22.80	Cos	921	23	103.2	7.6	57	45	2	(10) Kepler128c
277.01	16.23	Cos	448.57	0.51	120.2	1	20	78	2	(1), (2), (16) Kepler36c
277.02	13.85	Cos	439.4	1.9	180.1	6.8	58	72	2	(16) Kepler36b
282.01	27.51	Cos	469	20	2	0.73	2.5	46	3	(17) Kepler130c
289.01	26.63	Cos	120.2	3.3	2.3	2.4	5.1	44	2	
303.01	60.93	Cos	1490	150	5.1	1.5	4.6	21	1	
308.01	35.60	Cos	617.4	3.9	35.1	1.5	6.5	38	1	(2)
314.01	13.78	Cos	1209	92	4.06	0.74	4.5	96	3	(18) Kepler138c
314.02	23.09	Cos	1132	24	21	1.3	3.2	55	3	(18) Kepler138d
315.01	35.58	Pol	~115	...	10	38	1	
316.02	157.06	Cos	1008	84	28.6	8.4	8.9	7	3	(7) Kepler139c
318.01	38.58	Cos	885	14	11.9	0.81	4.3	32	1	
319.01	46.15	Cos	307.2	1.4	13.02	0.74	4.1	28	1	
345.01	29.88	Cos	956	25	11.5	0.74	2.7	34	1	
350.01	12.99	Pol	~45	...	13	75	1	
353.01	152.11	Pol	~3	...	1	8	2	
370.01	42.88	Cos	1670	120	20.3	3.8	9.4	29	2	(10) Kepler145c
372.01	125.63	Cos	445.4	1.1	14.03	0.25	12	10	1	
374.01	172.70	Cos	1388	84	37.8	6.2	5.7	7	1	
377.01	19.25	Cos	1349.74	0.48	523.93	0.53	35	64	3	(2),(19) Kepler9b

Table 5
(Continued)

KOI	Period ^a (days)	Model ^b	Period ^c (days)	σ_p^d (days)	Amp ^e (minutes)	σ_A^f (minutes)	Res ^g (minutes)	N ^h	Multiplicity ⁱ	References
377.02	38.96	Cos	1354.21	0.32	1189.8	0.76	81	33	3	(1), (2), (19) Kepler9c
410.01	7.22	Pol	~3.5	...	1.5	179	1	
417.01	19.19	Cos	304.3	8.8	1.05	0.8	1.7	64	1	
		Cos	202.6	3.2	0.96	0.26	1.7			
448.02	43.58	Pol	~200	...	50	26	2	(2), (7) Kepler159c
456.01	13.70	Cos	879	12	20.4	1.3	7.7	94	2	(2), (7) Kepler160c
457.02	7.06	Cos	280	3.4	7.98	0.98	8.1	149	2	(7) Kepler161c
464.01	58.36	Cos	482	11	3.93	0.59	0.93	21	2	
473.01	12.71	Cos	832	13	29.8	2.1	12	83	1	(2)
474.03	94.90	Cos	275.7	2.6	50	14	160	14	4	
		Cos	406.6	8.9	26.4	6.2	160			
500.01	7.05	Cos	189.8	1.7	8.5	1.6	5.7	85	5	(1),(10) Kepler80b
500.02	9.52	Cos	193.1	1.3	9.5	1.6	6.7	62	5	(1),(10) Kepler80c
509.03	39.61	Pol	~160	...	40	24	3	(7) Kepler171d
520.01	12.76	Cos	1294	54	19.1	2.2	8.6	96	3	(7) Kepler176c
520.03	25.75	Cos	1298	68	24.3	3.4	9.1	39	3	(7) Kepler176d
523.01	49.41	Pol	~10	...	5	25	2	(10) Kepler177c
524.01	4.59	Cos	334	1.7	17.03	0.91	8.3	273	1	(2)
525.01	11.53	Pol	~50	...	15	113	1	
528.02	96.68	Cos	1059	78	23.3	4.1	8.2	13	3	(7) Kepler178d
536.01	81.17	Cos	454	37	6.3	3.7	1.6	10	1	
564.01	21.09	Pol	~900	...	190	55	3	(1)
564.02	127.91	Pol	~40	...	15	9	3	
592.01	39.75	Cos	491.5	8.7	31.5	4.3	14	33	1	
598.01	8.31	Cos	559	16	9.1	1.3	12	145	2	(7) Kepler195b
620.01	45.16	Cos	790	12	7.91	0.41	2.5	29	3	(15) Kepler51b
620.02	130.18	Pol	~10	...	3	9	3	(20) Kepler51d
620.03	85.32	Cos	1100	70	16.2	3.2	11	12	3	(15) Kepler51c
622.01	155.04	Cos	799	61	4.7	2.2	2	9	1	
638.01	23.64	Pol	~100	...	10	45	2	(7) Kepler199b
652.01	16.08	Cos	225	5.5	0.86	0.4	1.6	73	1	
672.02	41.75	Cos	1061	76	9.2	2.4	7.8	30	2	(7) Kepler209c
676.01	7.97	Cos	738	18	2.04	0.23	1.7	122	2	(7) Kepler210c
700.01	30.86	Cos	620	39	5.5	2.2	7.5	38	4	(7) Kepler215d
709.01	21.39	Cos	1118	57	15.7	3.3	13	59	1	
720.03	18.37	Pol	~9	...	5	34	4	(7) Kepler221e
730.01	14.79	Cos	1292	78	61.6	9.1	20	38	4	(1), (7) Kepler223d
730.03	19.73	Cos	1690	100	108	16	49	40	4	(1), (7) Kepler223e
738.01	10.34	Pol	~55	...	20	92	2	(2),(21) Kepler29b
738.02	13.29	Pol	~80	...	25	67	2	(21) Kepler29c
746.01	9.27	Pol	~15	...	10	140	1	
757.02	41.20	Pol	~35	...	10	23	3	(7) Kepler229d
759.01	32.63	Cos	1248	21	57.8	2.9	4.4	31	2	(7) Kepler230b
760.01	4.96	Cos	1051	37	1.05	0.16	0.98	247	1	
775.02	7.88	Cos	205.5	1.3	16.2	1.6	11	113	3	(15) Kepler52b
784.01	19.27	Cos	515.6	9.6	20.9	2.5	15	50	2	(2), (7) Kepler231c
806.01	143.21	Cos	372.53	0.85	73.3	1.2	17	9	3	(2),(21) Kepler30d
806.02	60.33	Cos	968.9	3.5	33	0.55	4.3	21	3	(21) Kepler30c
806.03	29.32	Cos	984.87	0.62	1471.2	3.9	45	44	3	(2),(21) Kepler30b
811.01	20.51	Cos	968	79	4.1	1.4	6.4	62	1	
824.01	15.38	Cos	987	25	7.26	0.68	4.2	50	1	
829.01	18.65	Cos	554	20	11.7	3.3	13	56	3	(15) Kepler53b
829.03	38.56	Cos	496	14	22.6	3.7	17	30	3	(15) Kepler53c
834.01	23.65	Cos	382.3	6.8	4.66	0.7	3.5	56	5	(10) Kepler238e
841.01	15.34	Cos	723	10	15.3	1.3	7.1	84	3	(2),(14) Kepler27b
841.02	31.33	Cos	714.2	8.2	18.2	1.2	9	42	3	(14) Kepler27c
868.01	236.00	Cos	998.9	9.1	36.1	1.4	5.9	6	1	
869.02	36.28	Cos	595.8	7.5	65.6	3.8	23	31	4	(7) Kepler245d
870.01	5.91	Cos	230	2.4	7.1	1.3	8.6	193	2	(14) Kepler28b
870.02	8.99	Cos	230.4	2.7	11.5	2.1	12	115	2	(14) Kepler28c

Table 5
(Continued)

KOI	Period ^a (days)	Model ^b	Period ^c (days)	σ_P^d (days)	Amp ^e (minutes)	σ_A^f (minutes)	Res ^g (minutes)	N ^h	Multiplicity ⁱ	References
872.01	33.60	Cos	190.06	0.12	52.68	0.69	16	38	2	(2),(22) Kepler46b
877.02	12.04	Cos	536	12	9.3	1.5	10	88	3	(10) Kepler81c
880.01	26.44	Cos	969	32	21.5	2.8	10	50	4	(10) Kepler82b
880.02	51.54	Cos	1232	13	62.7	2.2	10	26	4	(10) Kepler82c
884.02	20.49	Cos	803.6	1	188.25	0.8	19	52	3	(1), (2), (7) Kepler247d
886.01	8.01	Cos	849.8	4.8	66.4	1.6	11	139	3	(2),(15) Kepler54b
886.02	12.07	Cos	852.1	5.5	124	3.4	15	78	3	(15) Kepler54c
902.01	83.93	Pol	~85	...	5	18	1	
904.02	27.97	Pol	~255	...	40	48	5	(15) Kepler55b
904.03	42.12	Pol	~225	...	60	29	5	(15) Kepler55c
918.01	39.64	Cos	865.4	8.1	6.34	0.2	1.4	31	1	(2)
928.01	2.49	Cos	117.56	0.18	31.5	1.2	13	368	1	(1)
935.01	20.86	Cos	941	13	22.8	1	5.3	62	4	(1),(21) Kepler31b
935.02	42.63	Cos	1162	42	22.2	3.1	6.2	26	4	(21) Kepler31c
952.01	5.90	Cos	267.1	4.3	6.8	1.5	9.3	136	5	(21) Kepler32b
984.01	4.29	Cos	2142	49	319	40	29	306	1	(2)
		Cos	578.9	1	62.69	0.54	29			
1061.01	41.81	Cos	1450	100	70	16	23	30	1	
1081.01	9.96	Cos	1010	12	73.8	2.5	17	114	1	(2)
1086.01	27.67	Cos	1630	150	20.7	4.3	13	46	1	
1102.01	12.33	Cos	413	6.7	43.8	6.1	33	75	4	(2),(12) Kepler24c
1102.02	8.15	Cos	439.7	7.7	30	4.5	25	103	4	(2),(12) Kepler24b
1103.01	90.12	Pol	~60	...	20	13	1	
1145.01	30.61	Cos	1802	20	507	11	26	42	1	(2)
1162.01	158.69	Pol	~15	...	2	7	1	
1203.03	48.65	Cos	824	40	79	14	33	14	3	(10) Kepler276d
1209.01	271.03	Cos	2480	370	3100	1400	100	5	1	
1215.01	17.32	Cos	348.3	7.8	20.6	5.7	23	68	2	(10) Kepler277b
1221.02	51.07	Cos	829	41	144	32	96	21	2	(7) Kepler278c
1236.01	35.74	Cos	1194	23	80.4	4.2	20	29	3	(7) Kepler279c
1236.03	54.41	Cos	1254	20	195.6	3.7	24	18	3	(10) Kepler279d
1241.02	10.50	Cos	541.9	6.2	180	17	100	87	2	(1),(15) Kepler56b
1242.01	99.64	Pol	~3	...	1	12	1	
1270.02	11.61	Cos	456	4.3	34.1	2.8	14	83	2	(2),(15) Kepler57c
1271.01	162.05	Pol	~85	...	40	7	1	(2)
1335.01	127.83	Cos	1083	91	6	2.1	2.4	10	1	
1353.01	125.86	Cos	1277	40	8.86	0.69	0.47	9	2	(7) Kepler289c
1355.01	51.93	Cos	124.5	1.3	6	2	6.2	24	1	
1426.01	38.87	Cos	1040	20	44	3.5	8.7	30	3	(7) Kepler297b
1426.02	74.93	Pol	~50	...	10	14	3	(7) Kepler297c
1426.03	150.03	Cos	1323	59	34.6	3.5	5.2	10	3	
1429.01	205.91	Cos	734	35	26.8	4.1	2.6	6	1	
1472.01	85.35	Cos	1440	160	4.1	1.2	2.3	17	1	
1474.01	69.73	Cos	643.8	1.2	39.04	0.54	25	13	1	(2),(23) Kepler419b
1476.01	56.36	Pol	~50	...	10	21	1	
1477.01	169.51	Pol	~50	...	10	4	1	
1478.01	76.14	Cos	1061	23	12	1.1	2	14	1	
1503.01	150.24	Cos	832	81	9.3	3.5	12	10	1	
1527.01	192.67	Pol	~20	...	3	6	1	
1529.01	17.98	Cos	623.4	8.6	84	6.7	25	61	2	(2),(15) Kepler59c
1546.01	0.92	Cos	144.94	0.13	1.503	0.041	1.4	1384	1	
1552.01	77.63	Cos	693	57	1.27	0.67	0.92	12	1	
1573.01	24.81	Cos	1457	14	82.1	1.3	4.8	47	2	(2)
1574.01	114.74	Cos	552	14	11	1.4	2.6	10	3	(24) Kepler87b
1576.01	10.42	Cos	517	24	4.2	1.4	8.4	117	3	(10) Kepler307b
1576.02	13.08	Cos	486	19	8.6	2.2	12	87	3	(10) Kepler307c
1581.01	29.54	Cos	938	17	91.8	6.4	30	42	2	(2)
1581.02	144.56	Cos	539	18	49.9	9.8	22	9	2	
1582.01	186.44	Cos	1014	49	55	11	2.4	6	1	
1596.02	105.36	Cos	1410	180	18.5	6.4	6.2	9	2	(7) Kepler309c

Table 5
(Continued)

KOI	Period ^a (days)	Model ^b	Period ^c (days)	σ_p^d (days)	Amp ^e (minutes)	σ_A^f (minutes)	Res ^g (minutes)	N ^h	Multiplicity ⁱ	References
1599.01	20.41	Cos	1483	36	202	15	28	53	2	(2)
1622.01	69.84	Cos	681	34	21	5	19	17	1	
1628.01	19.75	Cos	471	17	6.1	1.8	8.6	60	2	(7) Kepler312c
1675.01	14.62	Cos	532	18	14.2	3.2	14	66	1	
1685.01	70.47	Cos	1110	110	12.8	4.3	6.2	17	1	
1707.01	96.11	Pol	~60	...	30	12	2	(7) Kepler315b
1720.01	59.66	Pol	~45	...	20	21	1	
1751.02	21.00	Pol	~70	...	5	44	2	
1781.01	7.83	Pol	~3	...	2.1	97	3	
1781.03	58.02	Cos	922	17	39.8	2.4	9.8	11	3	
1783.01	134.48	Cos	1390	130	6.2	2.2	5.3	9	2	
1783.02	284.07	Pol	~40	...	15	4	2	
1790.01	130.36	Cos	697	10	28.8	2.5	7	8	1	
1792.01	88.41	Cos	269	3.7	5.6	1.1	2.7	14	2	
1802.01	5.25	Cos	230.9	1.4	7.34	0.64	5.6	246	1	
1830.02	198.71	Cos	940	110	8	3.6	3.6	8	2	
1831.01	51.81	Pol	~45	...	5	16	4	(7) Kepler324c
1831.03	34.19	Pol	~230	...	40	25	4	
1838.01	16.74	Pol	~10	...	4.2	66	1	
1840.01	7.04	Cos	1567	68	30.2	2.8	18	155	1	(2)
1848.01	49.62	Pol	~30	...	15	27	1	
1854.01	43.04	Cos	1520	140	25	4.4	7.9	23	1	
1856.01	46.30	Cos	1182	27	77.6	2.9	11	28	1	
1873.01	71.31	Pol	~20	...	8	11	2	(10) Kepler328c
1884.01	23.09	Pol	~425	...	10	38	2	
1902.01	137.86	Cos	924	71	5.4	1.4	2.2	9	1	
1907.01	11.35	Cos	603	16	12.6	1.9	12	93	1	
1934.01	28.78	Cos	348.6	5.4	15.5	2.2	12	48	1	
1938.01	96.92	Cos	597	73	4.6	3.2	6.7	13	1	
1955.02	39.46	Pol	~40	...	20	31	4	(7) Kepler342d
1955.04	26.23	Cos	563	27	15.3	4.4	19	38	4	(7) Kepler342c
1973.01	3.29	Cos	408.2	5.1	18.6	2.4	12	211	1	
1989.01	201.12	Pol	~15	...	8	6	1	
2038.01	8.31	Cos	1091	42	38.9	6.0	28	75	4	(10) Kepler85b
2038.02	12.51	Cos	1008	28	59.9	4.3	33	67	4	(10) Kepler85c
2061.01	14.10	Cos	1269	24	151.1	5.6	26	76	2	
2086.02	8.92	Cos	715	28	29.4	7.2	35	100	3	(15) Kepler60c
2092.01	57.69	Cos	1270	130	22.6	5.7	10	20	3	(7) Kepler359c
2094.01	42.43	Cos	1510	130	43.2	6.8	19	28	2	
2199.01	9.03	Pol	~50	...	25	69	1	
2217.01	37.80	Pol	~10	...	30	29	1	
2283.01	17.40	Cos	331.2	8.2	22	15	26	53	1	
		Cos	521	31	16.6	6.5	26			
2291.01	44.30	Pol	~50	...	20	27	1	
2298.01	16.67	Cos	366	16	25.5	8.9	40	47	1	
2310.01	16.46	Pol	~15	...	15	61	1	
2386.01	16.27	Cos	1360	120	36.4	9.3	29	45	1	
2445.01	47.37	Cos	1089	44	79	11	18	17	1	
2603.01	73.71	Cos	1130	110	44	12	32	16	1	
2613.01	51.57	Cos	1530	130	52	10	17	21	1	
2666.01	64.03	Pol	~75	...	30	14	1	
2672.01	88.51	Cos	1303	11	58.61	0.53	3.1	12	2	(10) Kepler396c
2672.02	42.99	Cos	1518	31	32.4	1.5	3.4	29	2	(10) Kepler396b
2679.01	110.76	Cos	964	49	3.73	0.59	2.2	12	1	
2681.01	135.50	Cos	757	19	20.6	3.2	1.7	9	2	(7) Kepler397c
2691.01	97.45	Cos	1343	62	76	10	13	13	1	
2720.01	6.57	Cos	765	16	44.7	3.5	25	130	1	
2975.01	175.33	Cos	960	110	21.4	9.2	7.1	7	1	
3057.01	29.73	Cos	791	44	24.7	8.5	21	29	2	(7) Kepler405c
3072.01	24.34	Pol	~55	...	28	33	1	

Table 5
(Continued)

KOI	Period ^a (days)	Model ^b	Period ^c (days)	σ_P^d (days)	Amp ^e (minutes)	σ_A^f (minutes)	Res ^g (minutes)	N ^h	Multiplicity ⁱ	References
3375.01	47.06	Cos	1166	82	46.4	9.8	13	22	1	
3396.01	36.26	Pol	~130	...	90	22	1	
3481.01	32.71	Pol	~250	...	90	27	1	
3583.01	210.31	Pol	~1.0	...	0.05	5	1	
3602.01	249.36	Pol	~0.5	...	0.3	6	1	
3678.01	160.88	Cos	402.7	3.2	7.51	0.49	0.38	8	1	
3683.01	214.31	Cos	1219	84	7.83	0.89	3.2	7	1	
3692.01	1.16	Pol	~5	...	2	1032	1	
3720.01	213.40	Pol	~1	...	0.4	6	1	
3781.01	2.88	Cos	836.4	2.1	5.979	0.077	4.9	431	1	
4007.01	11.49	Pol	~90	...	45	70	1	
4014.01	234.24	Pol	~35	...	7	6	1	
4066.01	126.56	Cos	1640	110	81	17	21	11	1	
4307.01	160.85	Pol	~100	...	4	7	1	
4519.01	148.56	Cos	655	16	64.3	6.8	1.5	8	1	
4548.01	61.08	Cos	557	14	190	25	71	12	1	
4636.01	122.73	Cos	932	69	48	15	9.1	6	1	
4928.01	3.29	Cos	110.25	0.94	2.12	0.68	1.7	83	1	
5052.01	155.05	Cos	456	12	36.4	4	7.4	8	1	
5078.01	194.90	Cos	577	17	50.5	6.8	14	7	1	
5208.01	186.54	Pol	~165	...	50	6	1	
5210.01	125.95	Cos	888	28	216	36	41	7	1	
5453.01	190.65	Cos	1145	11	466	21	2.7	5	1	
5611.01	209.22	Cos	1051	35	66.1	7.5	5.8	6	1	
5651.01	83.49	Pol	~85	...	25	10	1	
5866.01	102.31	Cos	1132	75	70	12	11	10	1	

Notes.^a Orbital Period.^b Model type: “Cos” represents a cosine superimposed on a linear trend, “Pol” represents a parabolic fit, while “...” means no fit.^c Best-fit period of the O-C data using model Cos.^d Period uncertainty.^e The amplitude of the cosine fit.^f Amplitude uncertainty.^g Residual scatter (1.483 times their MAD).^h Number of TT measurements.ⁱ Number of detected planets in the system (see B12).

References. (1) Ford et al. (2011), (2) Ford et al. (2012b), (3) Van Eylen et al. (2014), (4) Ballard et al. (2011), (5) Weiss et al. (2013), (6) Marcy et al. (2014), (7) Rowe et al. (2014), (8) Cochran et al. (2011), (9) Nesvorný et al. (2013), (10) Xie (2014), (11) Lissauer et al. (2011a), (12) Ford et al. (2012a), (13) Deleuil et al. (2014), (14) Steffen et al. (2012a), (15) Steffen et al. (2013), (16) Carter et al. (2012), (17) Wang et al. (2014), (18) Kipping et al. (2014), (19) Holman et al. (2010), (20) Masuda (2014), (21) Fabrycky et al. (2012), (22) Nesvorný et al. (2012), (23) Dawson et al. (2014), (24) Ofir et al. (2014).

interested only in getting the best template to fit the light curve and not in analyzing the physical parameters of the system, we accepted limb-darkening parameters even if they were out of the range allowed by the theory of stellar atmospheres.

Because of the astrophysical basis of the Mandel–Agol model—in contrast to the other two which were merely mathematical heuristics, we preferred the Mandel–Agol model whenever it gave a good enough fit. Hence, we chose the Mandel–Agol model even in cases where its rms exceeded those of the other two models by up to 7%. More details about the three models can be found in Mazeh et al. (2013).

For most KOIs, the pipeline selected the Mandel–Agol model (2579 KOIs). The pipeline chose the Legendre-based model when there was a significant asymmetry in the folded light curve of the transit (17 KOIs). The Fermi-based model was selected only when the SNR of the folded light curve was too low (3 KOIs).

2.3. Deriving the Timing, Duration, and Depth of Each Transit

In order to derive the timing of a specific transit, we first searched through a grid of timings around the expected transit time, with a resolution of either one minute, or the estimated transit time uncertainty divided by five—whichever is lower. The transit time uncertainty was approximated to be (100 minutes)/(SNR of individual transit) (Mazeh et al. 2013, see also Figure 2). For each time shift on the grid we fitted the data with the KOI’s transit model, while keeping the duration and depth fixed. The grid point with the lowest χ^2 served as a first guess for the transit time.

In our next step we divided the transits into two groups. Group 1 consisted of KOIs whose transits had a duration longer than 1.5 hr and an SNR per transit larger than 10. (The SNR per transit was defined as the transit depth of the model divided by the median uncertainty of the individual points of the light curve and multiplied by the square root of the typical number

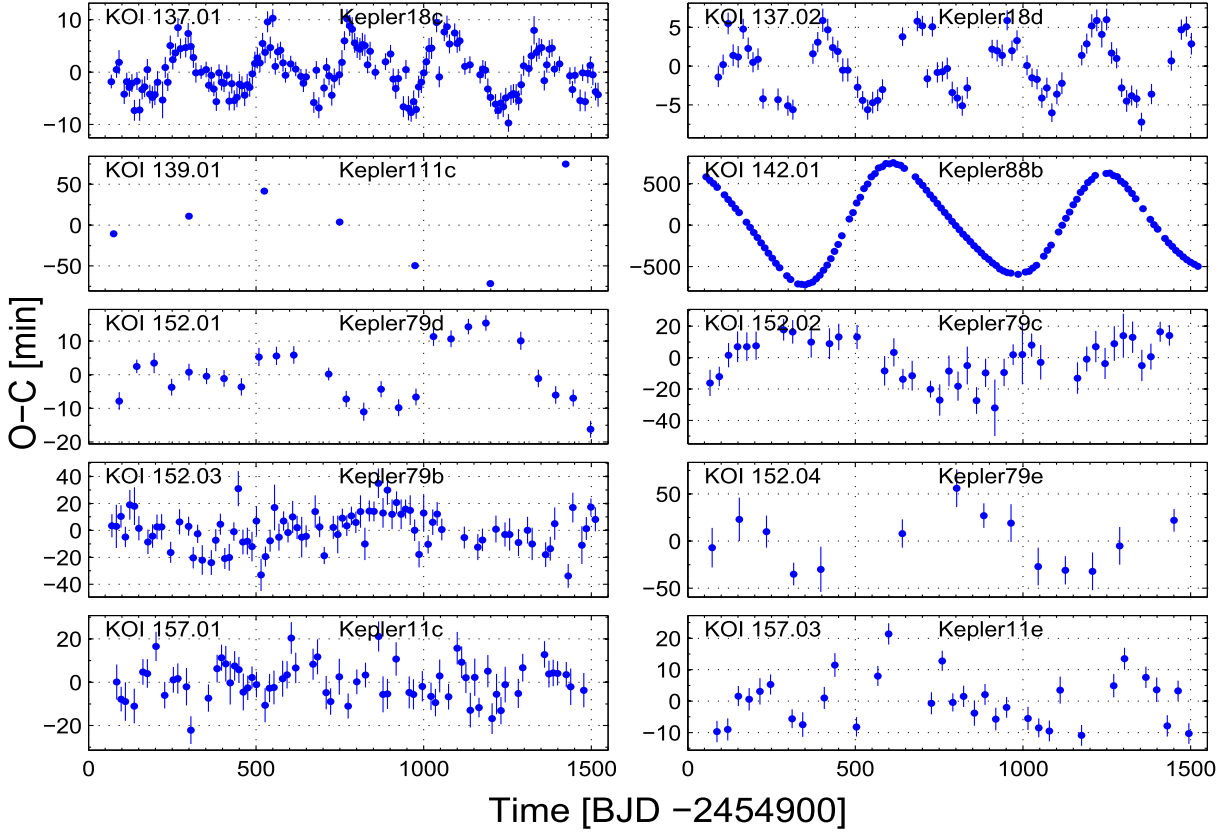


Figure 4. KOIs with significant long-term TTVs.

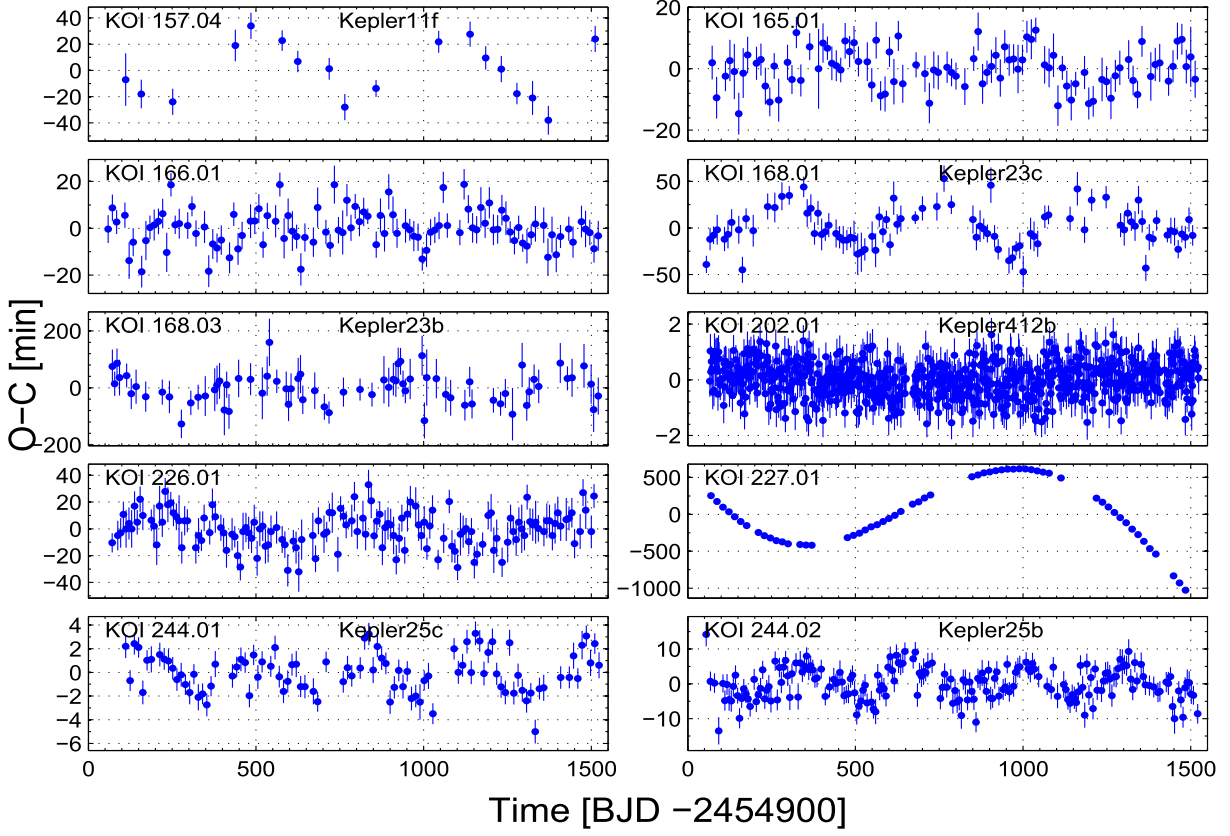


Figure 5. KOIs with significant long-term TTVs.

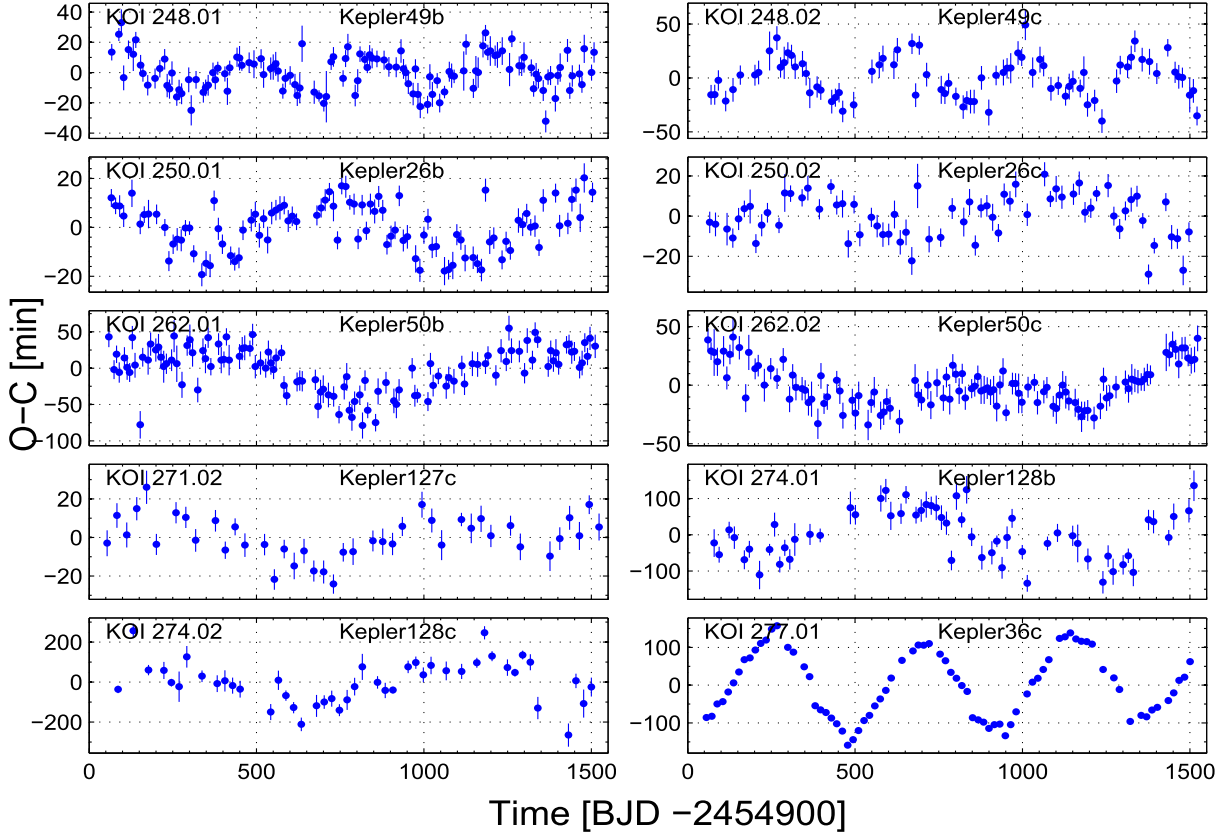


Figure 6. KOIs with significant long-term TTVs.

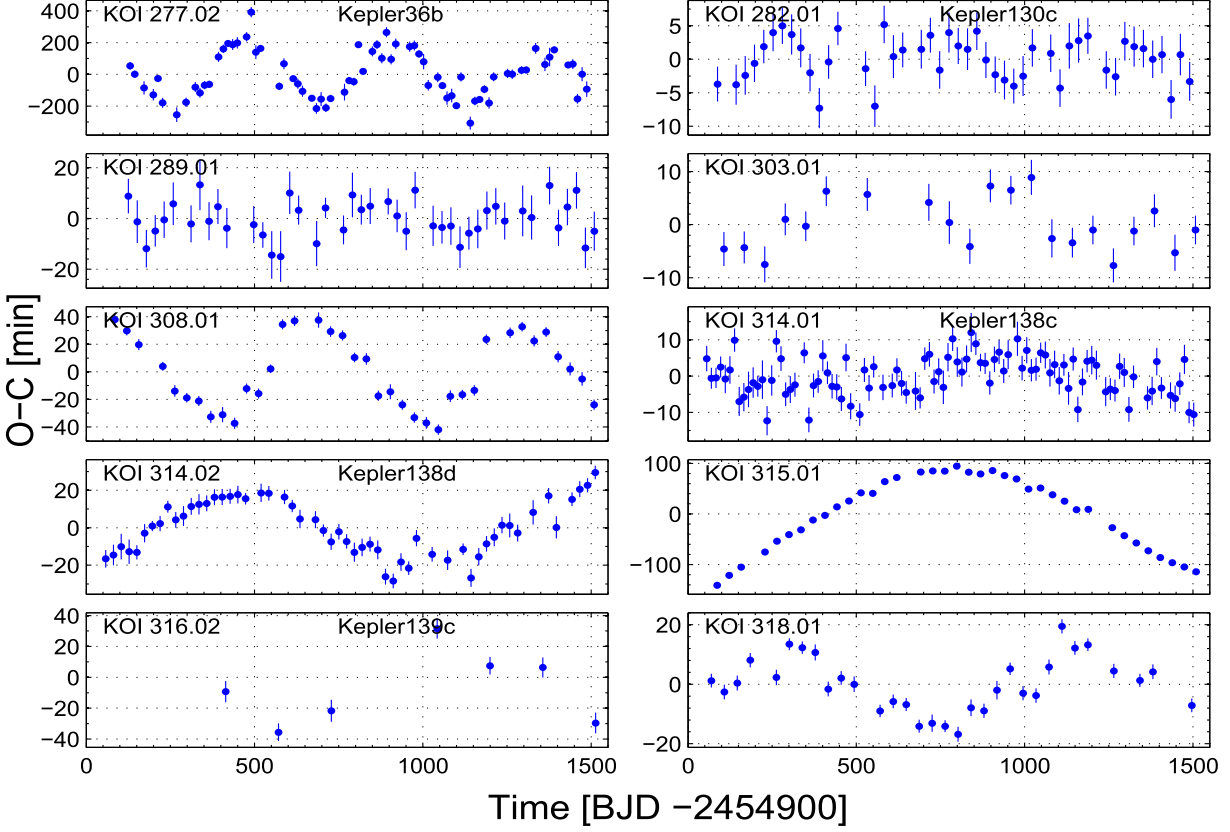


Figure 7. KOIs with significant long-term TTVs.

of measurements during one transit, including its ingress and egress.) Group 2 consisted of all other KOIs, which did not follow at least one of these two criteria. For both groups we performed a fine search for the best estimate of the transit timing, using MATLAB’s FMINSEARCH function, which is based on the Nelder–Mead simplex direct search, allowing the duration and depth of the transit to vary in group 1, while in group 2 only the timing was varied.

For KOIs of group 1, we define the TDV and TPV of each transit as the *relative* change of the duration and depth found for that transit, respectively, with respect to the duration and depth of the transit model. Deriving the template depends on the folded light curve, which in turn is based on the adopted transit timings. Therefore, fitting of the model was performed only after the first derivation of the timings for each KOI, and then we derived a new set of timings with the new improved template. This process converged after three iterations.

We estimated the uncertainties of the three quantities (when available) from the inverted Hessian matrix, calculated at the identified minimum. The uncertainty of each individual *Kepler* measurement of a KOI was derived from the scatter of the light curves around the polynomial fit before and after all transits of that planet. When the Hessian matrix turned out to be singular, we assigned an uncertainty that was equal to the median of the other uncertainties derived for the KOI in question. Whenever this was the case, we marked the error with an asterisk in the table of transit timings (see Table 3).

In order to verify the obtained uncertainties for the transit timings, we computed for 2339 KOIs, which had at least 7 transit timings, the scatter of their O-C values, $s_{\text{O-C}}$, defined as 1.4826 times the median absolute deviation (MAD) of the O-C series. We then compared this quantity with the typical error of each KOI, defined as the median of its timing uncertainties — $\bar{\sigma}_{\text{TT}}$. These two parameters should not be sensitive to timing and uncertainty outliers (see Table 3).

We expected the estimated scatter and the mean uncertainty values to be similar for systems with no significant TTV. This was indeed the case for most KOIs, as seen in Figure 1. KOIs with O-C scatter substantially larger than the typical timing uncertainty had significant TTVs (see below for a detailed analysis of those systems).

Mazeh et al. (2013) found that for each KOI $\bar{\sigma}_{\text{TT}} \sim (100 \text{ minutes})/\text{SNR}$. Figure 2 shows that this relation still holds.

2.4. Outliers and Overlapping Transits

We labeled a transit as an outlier if it did pass one of the following five tests:

1. Significance—We performed an F -test to compare the transit model, with the identified timing (and duration and depth when appropriate) found, against a constant flux assumption (no transit at all). We rejected all transits with an F -test p -value larger than 0.025. We have found 60,856 such transits.
2. Moving local outlier—We considered each transit with respect to its ten neighboring transits, fitting a parabola through five O-Cs before and another five after the transit. We labeled a transit timing as an outlier if its O-C deviated from the parabolic model by more than five times the parabola rms residuals plus three times the median error of the O-C of that KOI. The scatter was

calculated as $1.4826 \times \text{MAD}$ of the residuals. We have found 3336 such transits.

3. Global TTV outlier—A transit timing was labeled as an outlier in one out of two cases. The first was when its O-C deviated from the median of the O-Cs of that KOI by at least five times their scatter plus three times their median error. The second case was when its O-C deviated from the median of the O-Cs of that KOI by more than some factor η times the scatter of the O-Cs, $\bar{\sigma}$. The factor η we used depended on the total number of derived O-Cs of that KOI, N , such that we did not expect even one measurement to fall at random at a distance larger than $\eta\bar{\sigma}$ from the median of the O-Cs of that KOI, if the O-Cs were randomly distributed. We used $N \leq 100$, even for systems with larger number of points. We have found 23,030 such outlier transits.
4. TDV global outlier—A transit was labeled as an outlier when its TDV deviated from zero by at least five times the scatter of all TDVs of that KOI plus three times their median error. We have found 195 such transits.
5. TPV global outlier—A transit was labeled as an outlier when its TPV deviated from zero by at least five times the scatter of all TPVs of that KOI plus three times their median error. We found 192 such transits.
6. TTV, TDV, or TPV uncertainty outlier—A transit was labeled as an outlier when either its TTV, TDV, or TPV uncertainty deviated from the corresponding median of the other transit uncertainties of that KOI by at least eight times their scatter. We have found 2851 such transits.

All six types of outliers are noted in the catalog of the transit timings (Table 3; see below), by numbers that reflect their appearance in the list above. The Global TTV outlier procedure is an efficient approach to remove incorrect identifications, assuming there are no significant TTVs. For KOIs with significant TTVs this assumption does not hold, and therefore we sometimes had to undo this stringent outlier procedure for selected measurements that were obviously correct. We undid a total of 68 TTVs in 36 KOIs, which led to a total of 22,962 measurements that were labeled as global TTV outliers.

We also marked and ignored transits of multiple-planet systems when the transits of two or more planets “overlapped.” A transit was considered to be overlapped by another planet whenever the difference between their expected timings was smaller than twice the duration of that transit plus one duration of the interfering transit. We used twice the duration of the analyzed transit since that is the range over which the detrending fit was performed. However, we did not mark transits that were overlapped by another transit, if the overlapping transit had a transit duration multiplied by its depth smaller than 0.25 of the corresponding product of the analyzed transit. It seemed that in those cases the overlapping transits did not induce large TTV errors. We have found a total of 11,910 overlapped transits.

After marking the outliers and overlapped transits, we were left with 150,051 transits with derived timings only, and 64,121 ones for which we derived the timing, duration and depth.

2.5. The Catalog

We present our results in two tables, available at: ftp://wiseftp.tau.ac.il/pub/tauttv/TTV/ver_112. Table 2 lists the modified ephemerides of the KOIs, based on our analysis, together

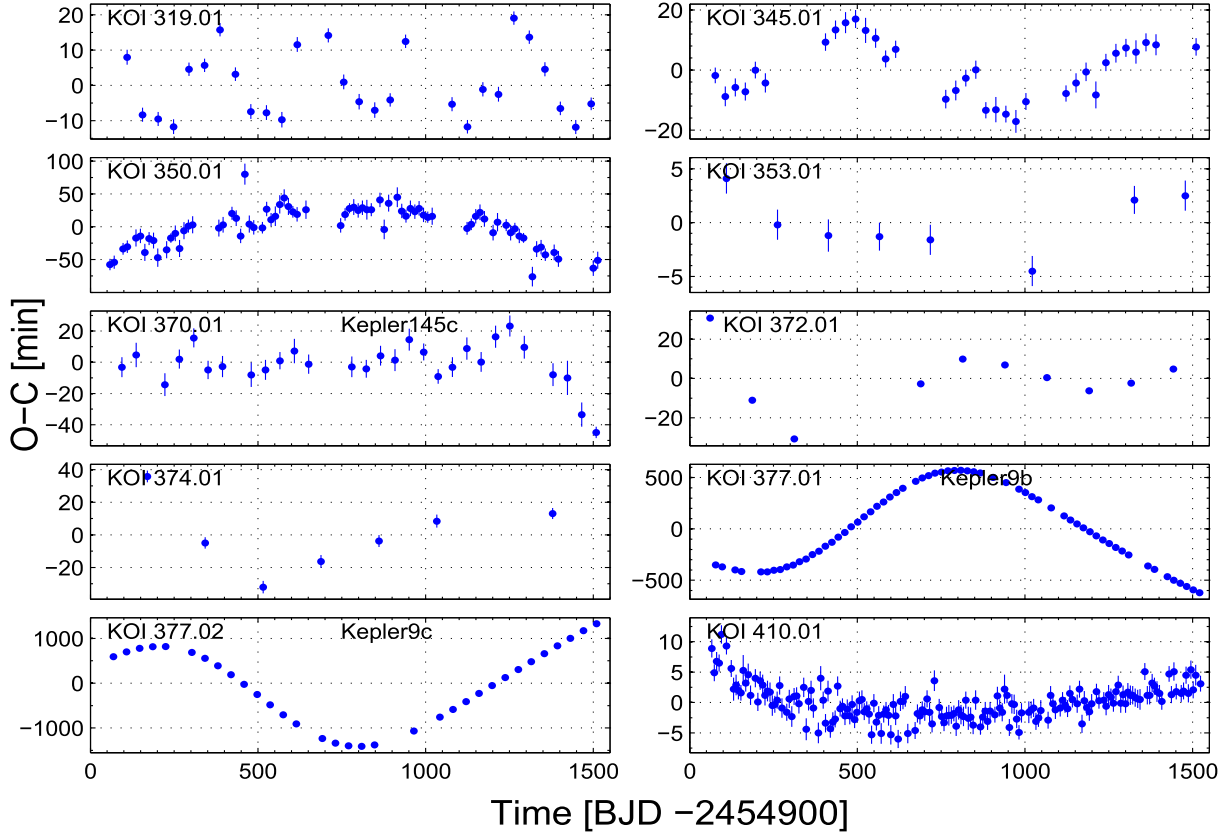


Figure 8. KOIs with significant long-term TTVs.

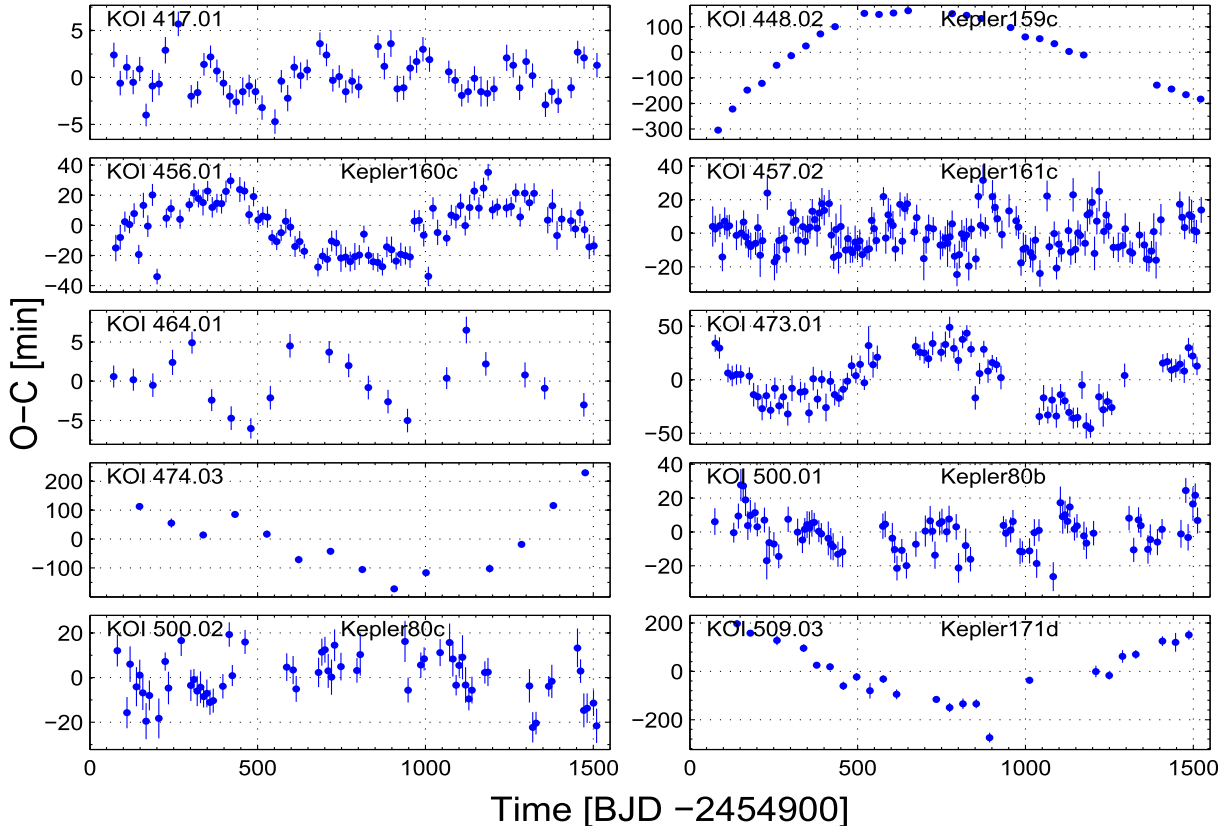


Figure 9. KOIs with significant long-term TTVs.

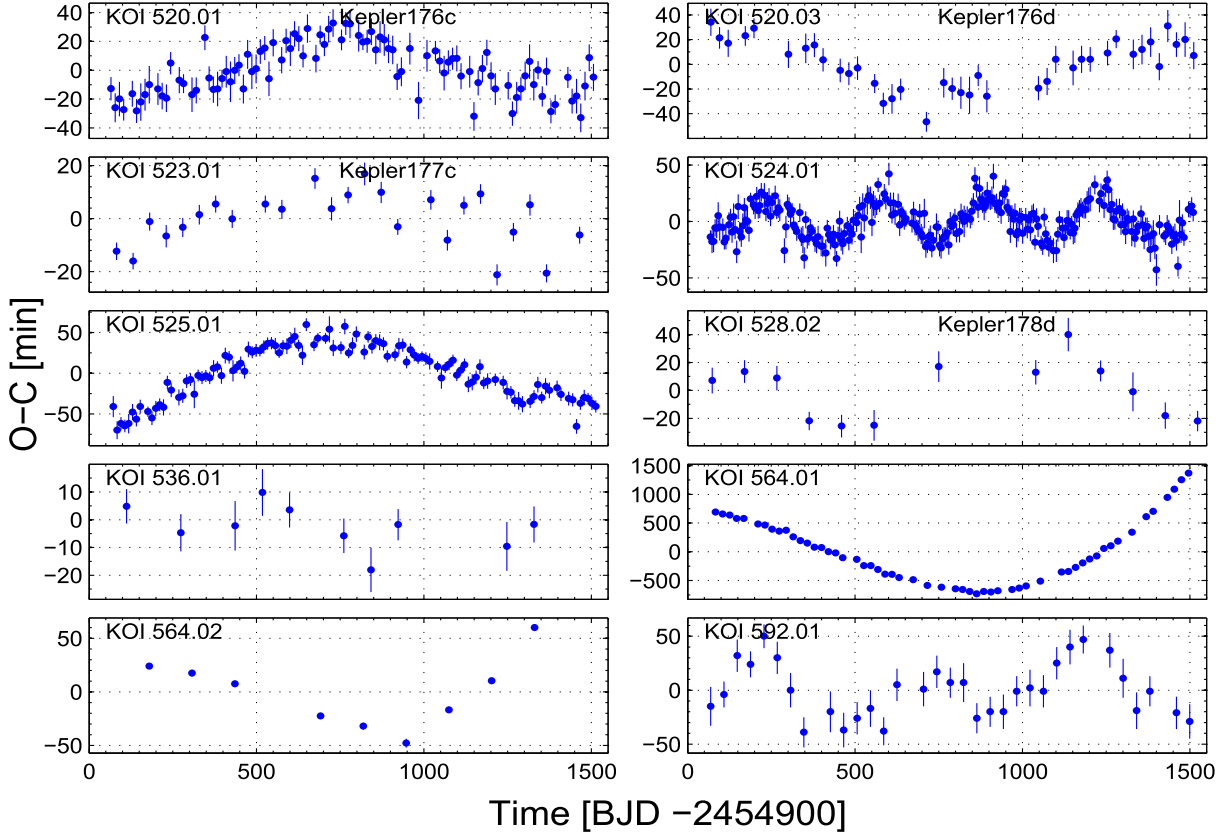


Figure 10. KOIs with significant long-term TTVs.

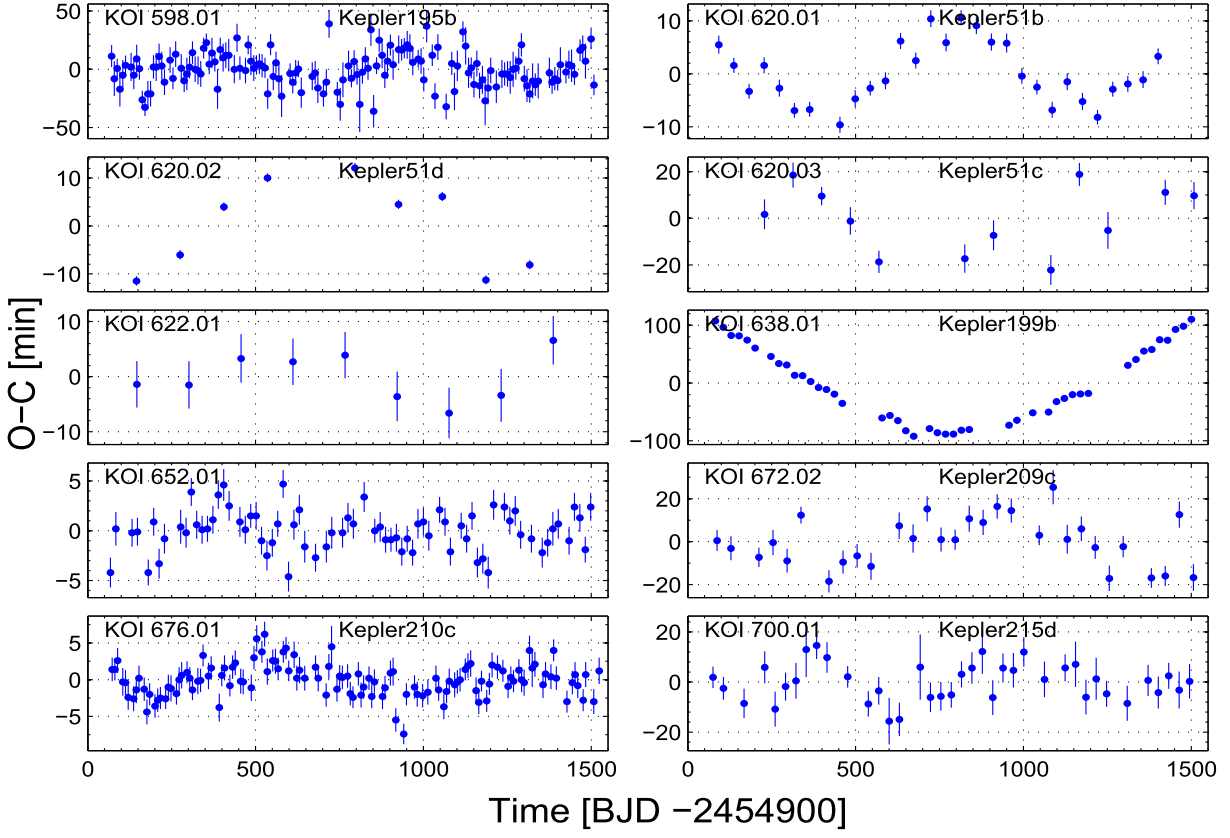


Figure 11. KOIs with significant long-term TTVs.

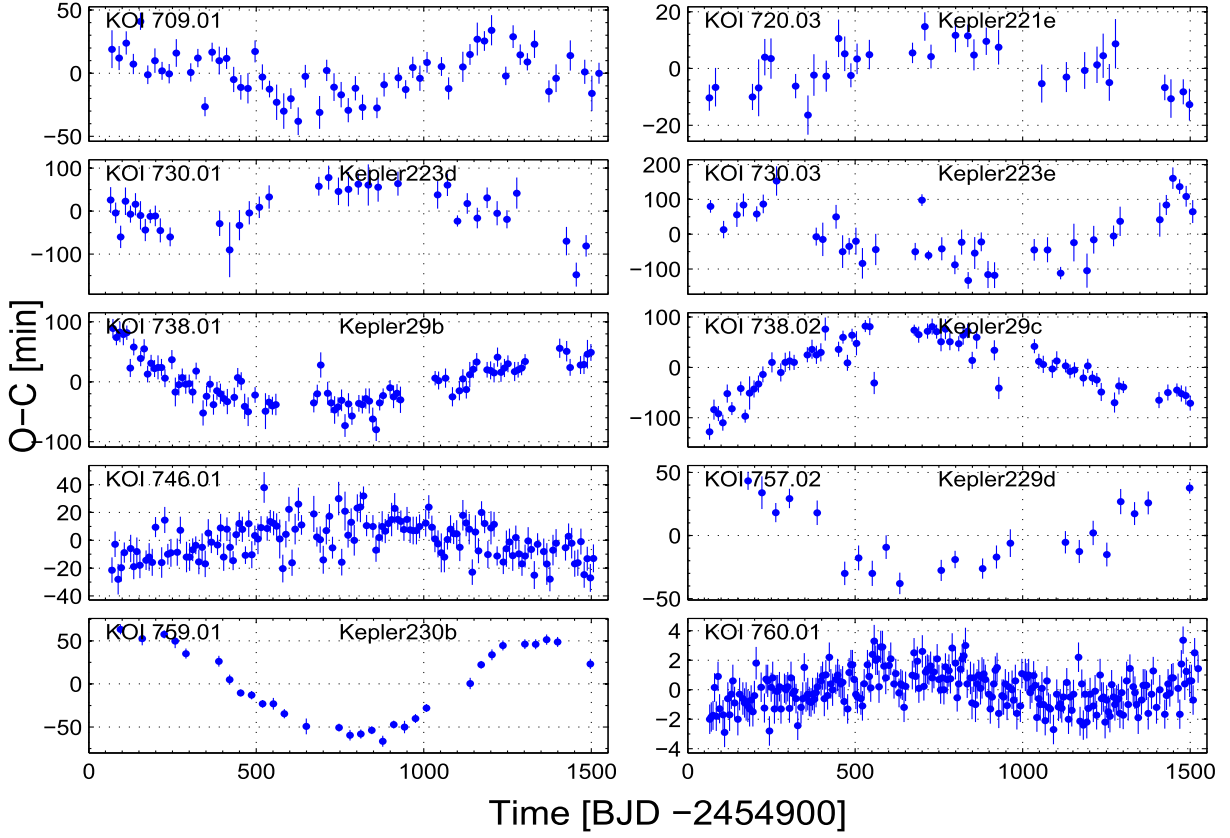


Figure 12. KOIs with significant long-term TTVs.

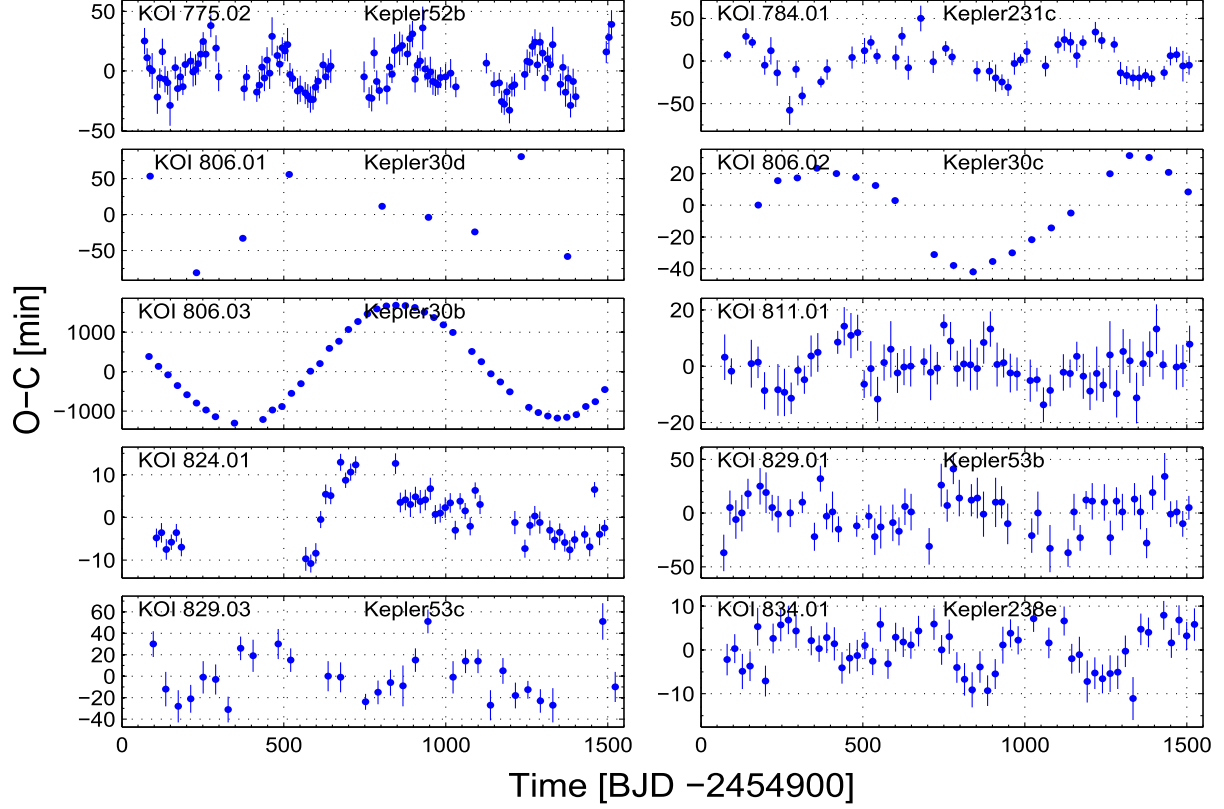


Figure 13. KOIs with significant long-term TTVs.

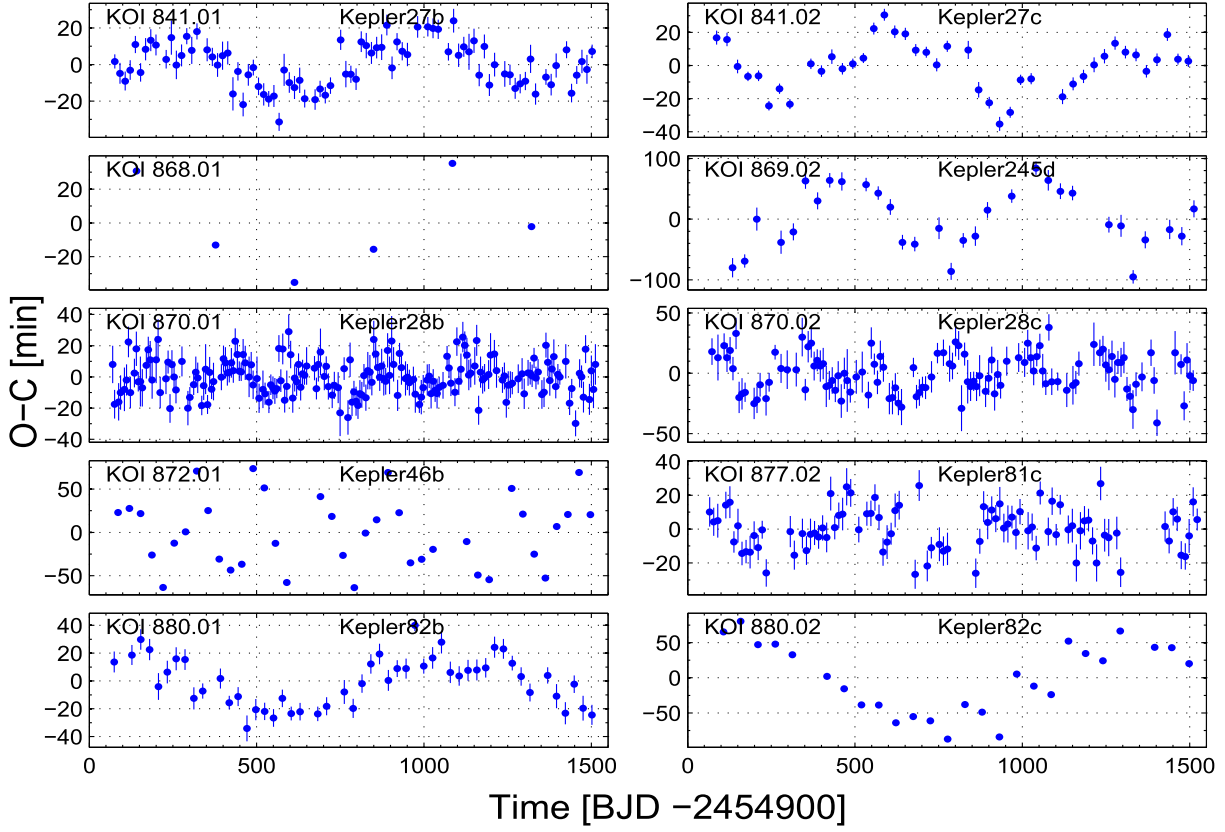


Figure 14. KOIs with significant long-term TTVs.

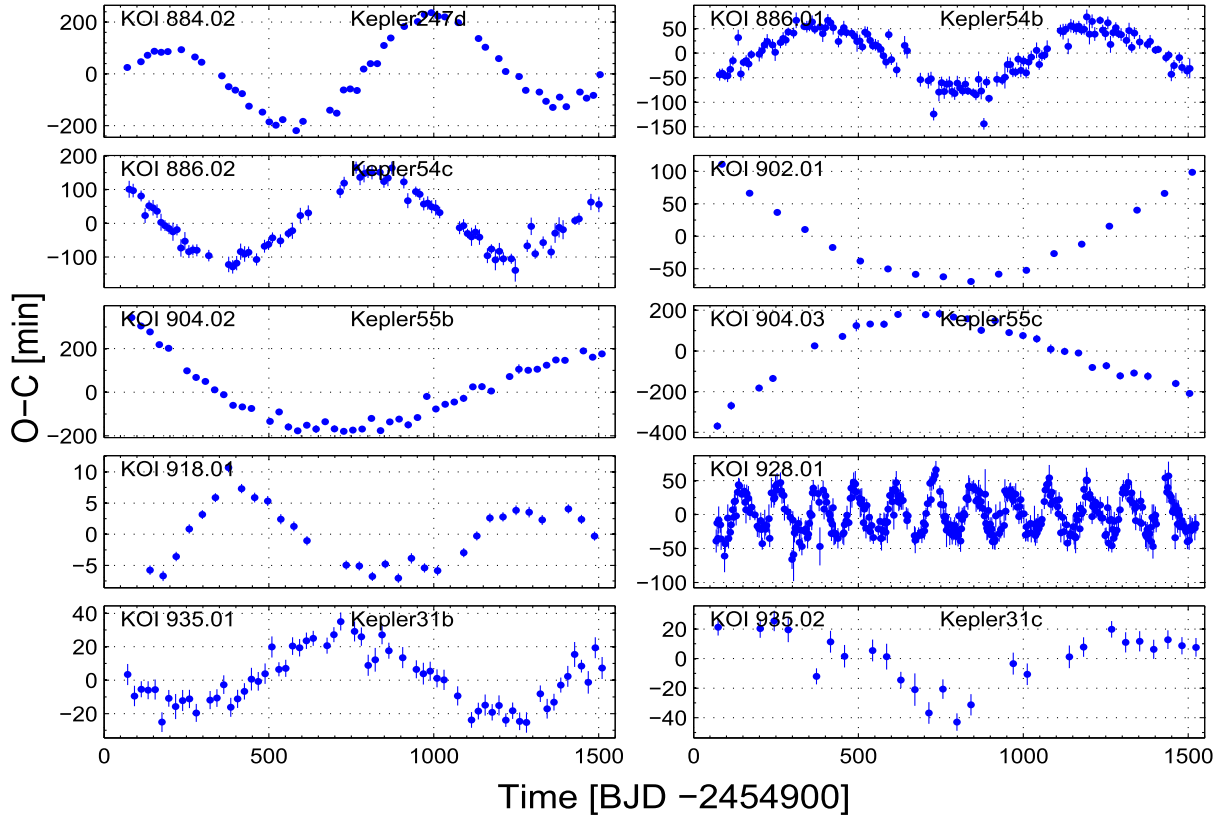


Figure 15. KOIs with significant long-term TTVs.

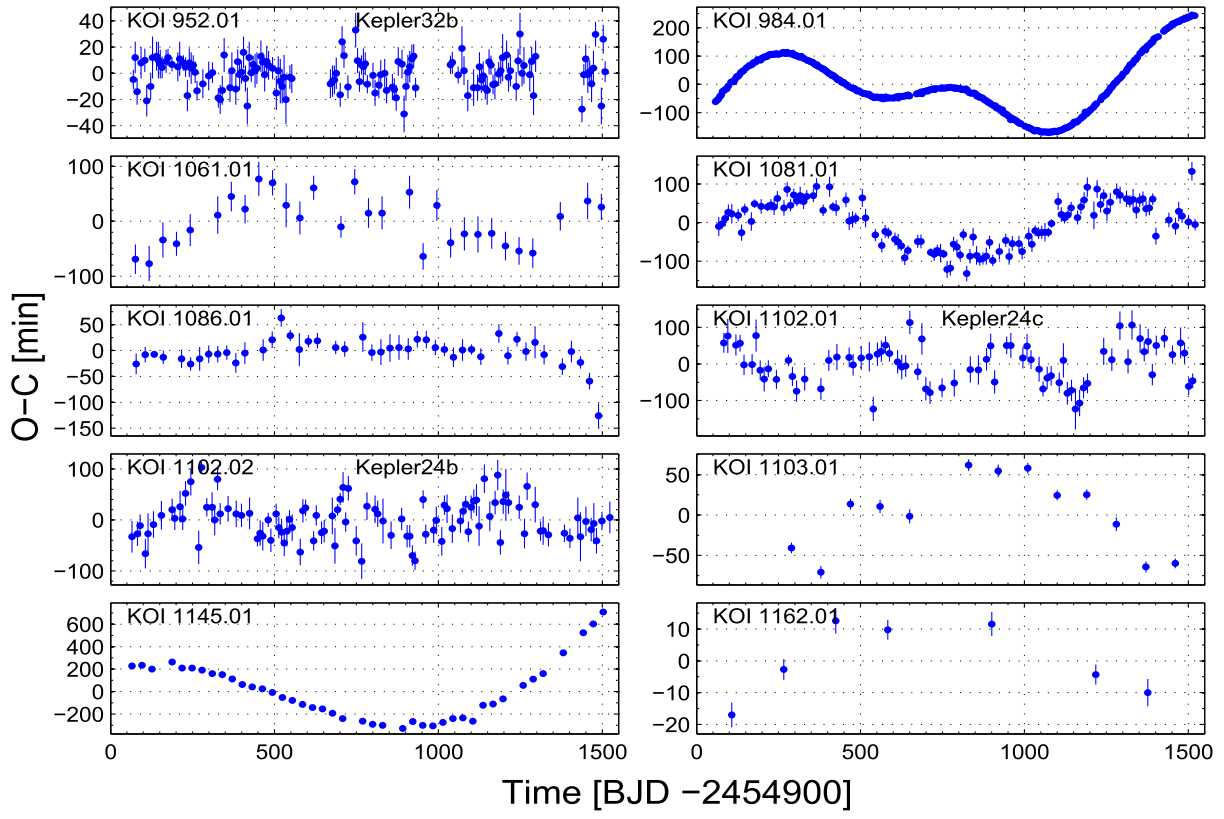


Figure 16. KOIs with significant long-term TTVs.

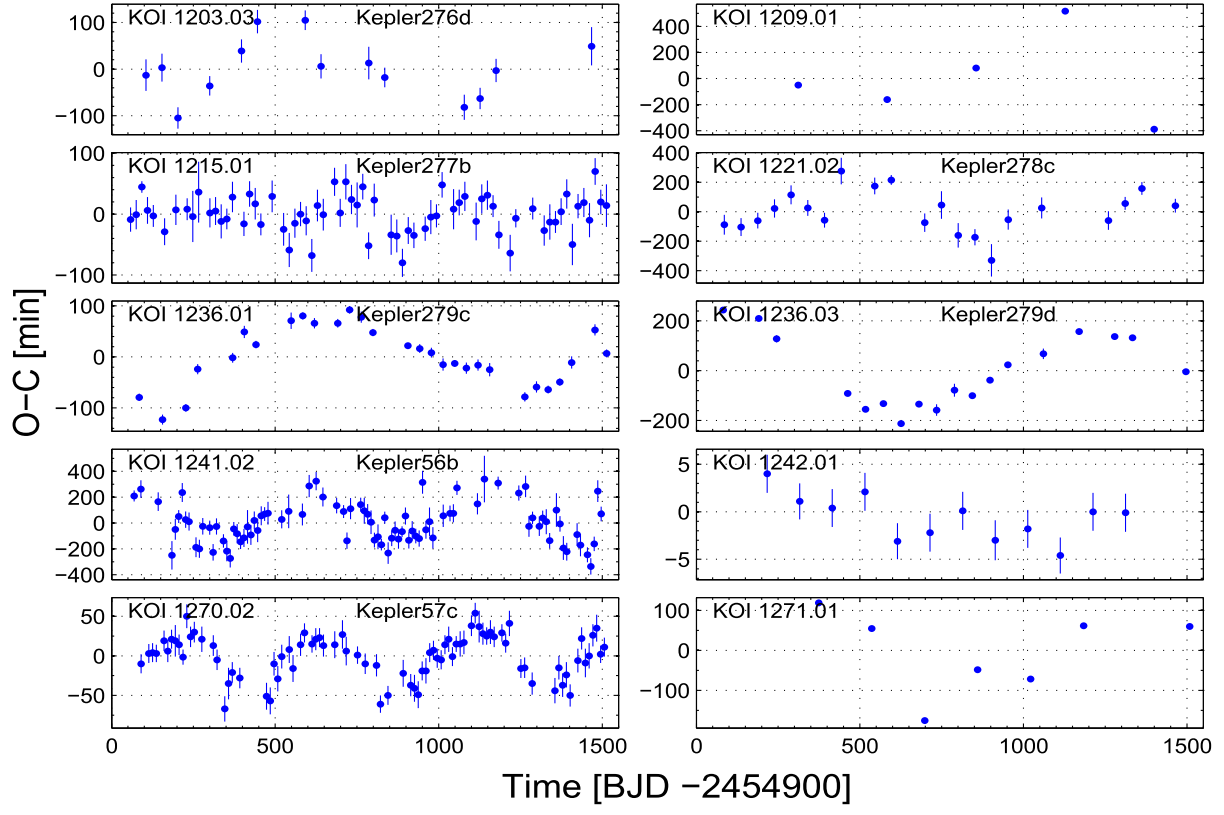


Figure 17. KOIs with significant long-term TTVs.

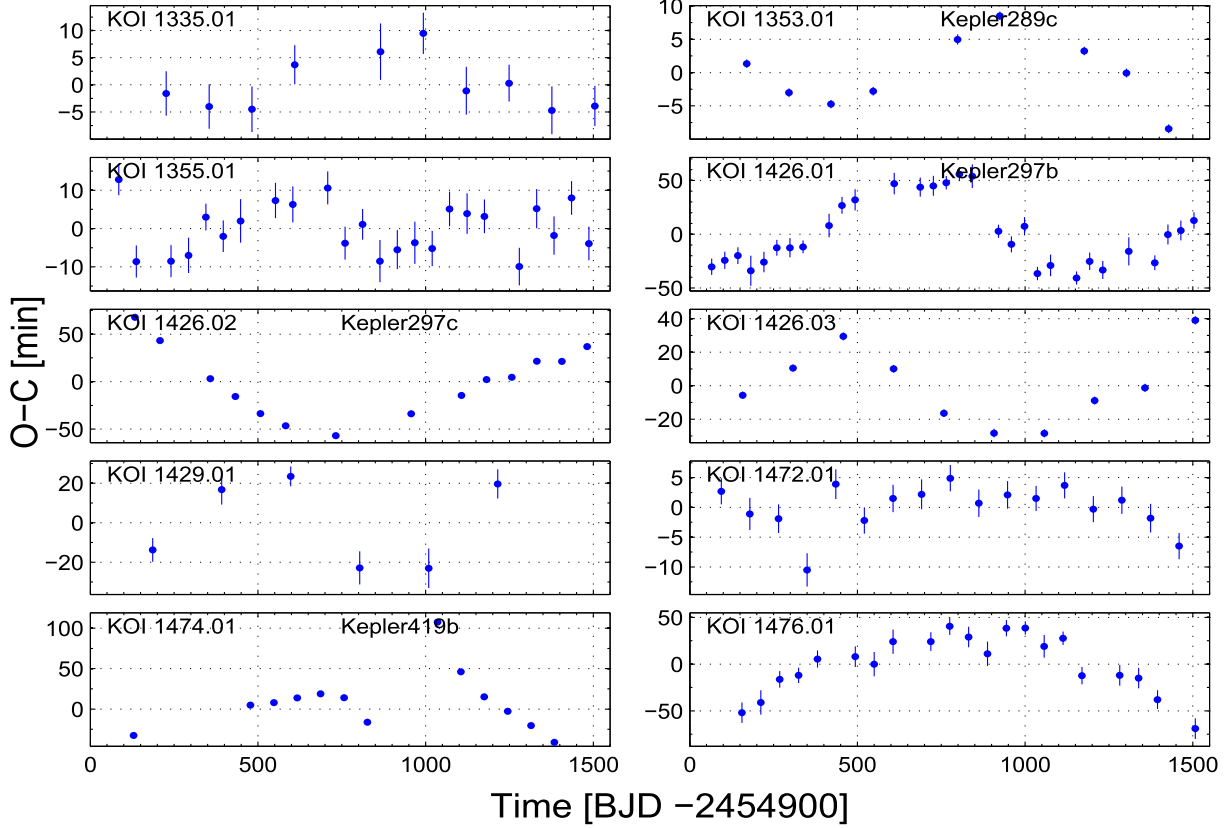


Figure 18. KOIs with significant long-term TTVs.

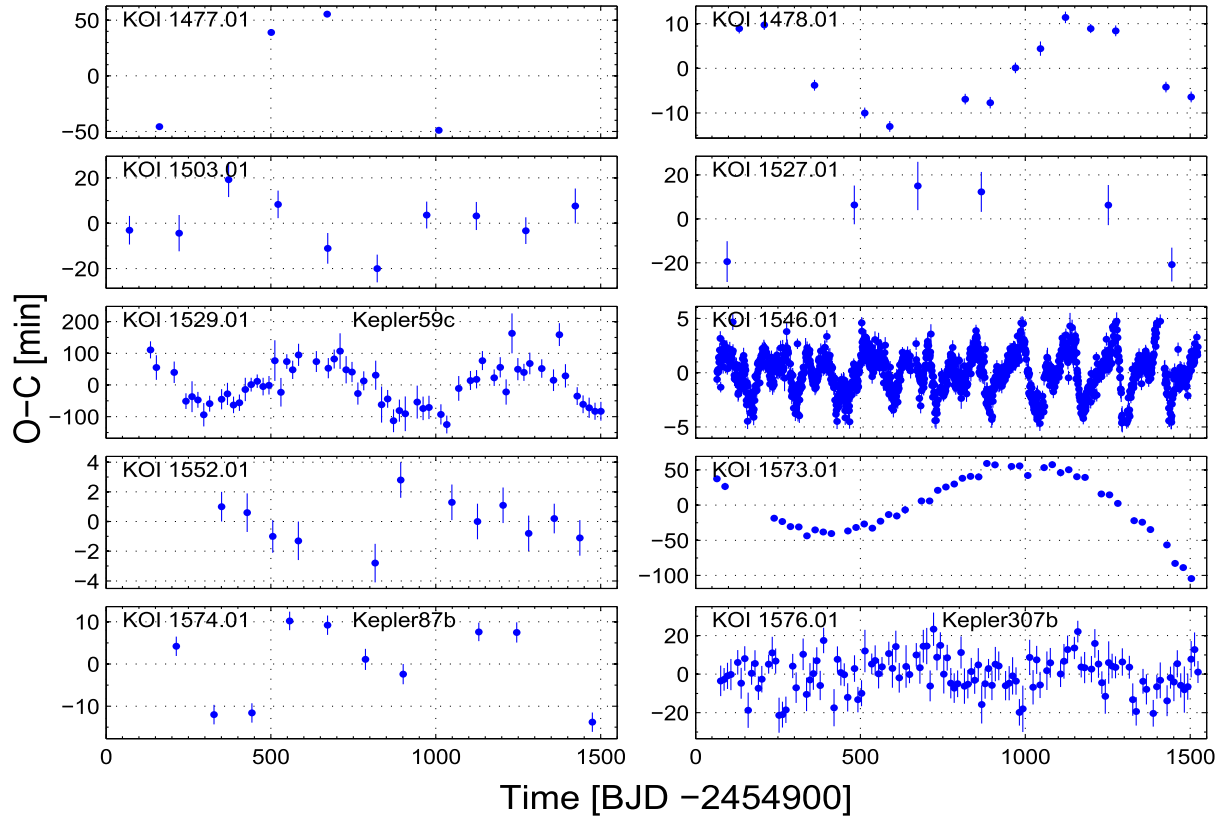


Figure 19. KOIs with significant long-term TTVs.

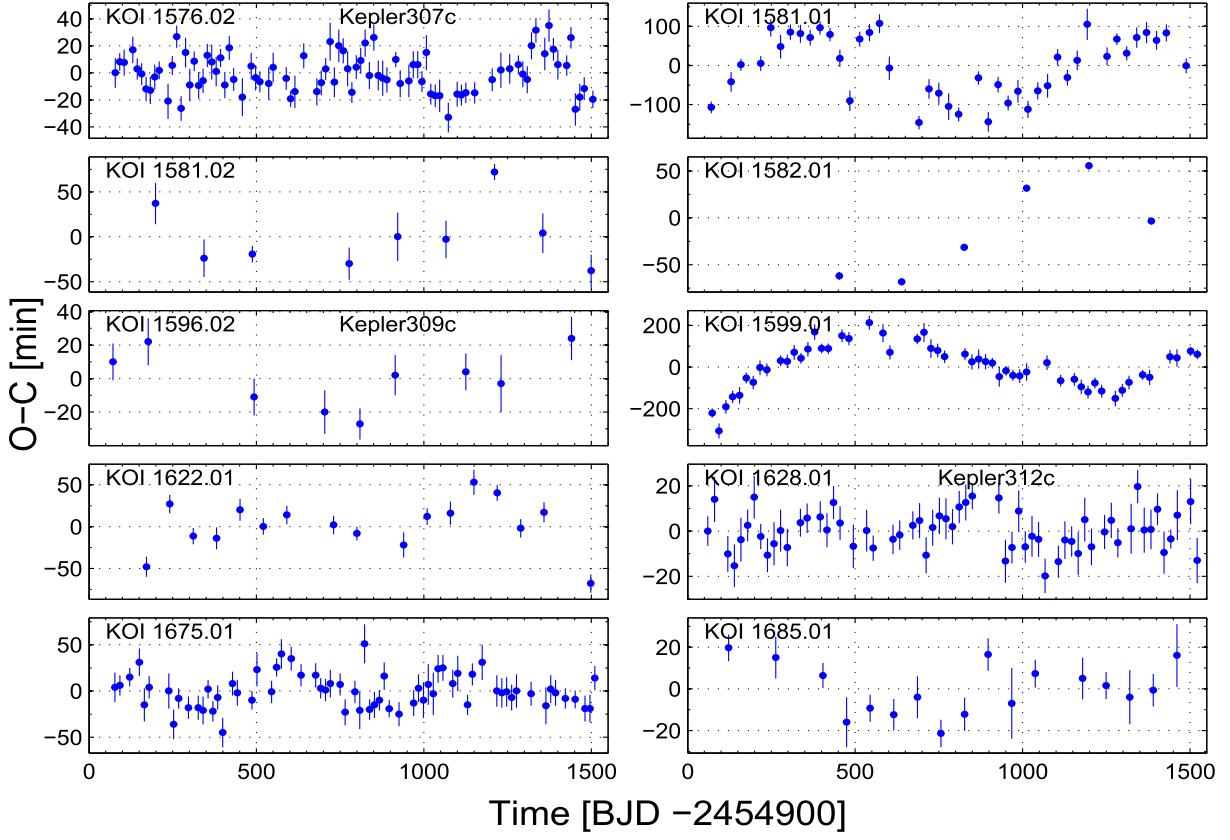


Figure 20. KOIs with significant long-term TTVs.

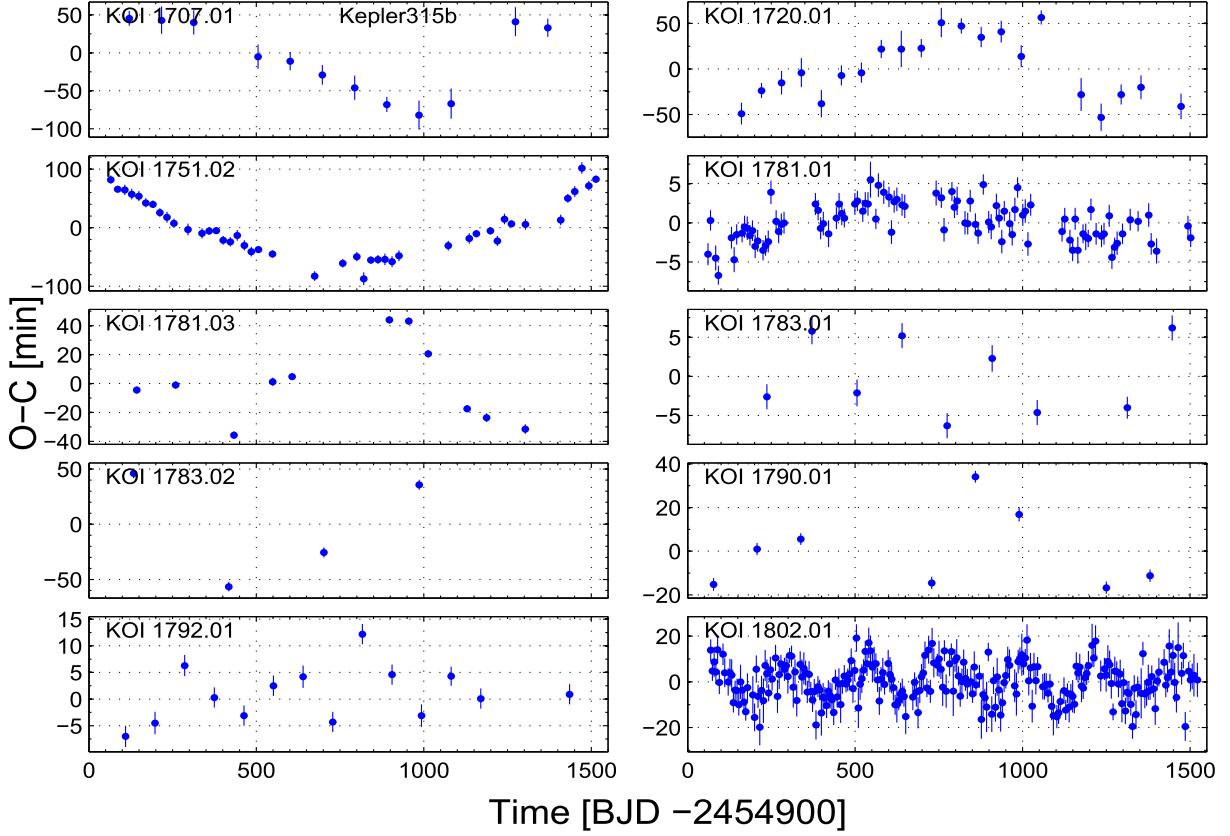


Figure 21. KOIs with significant long-term TTVs.

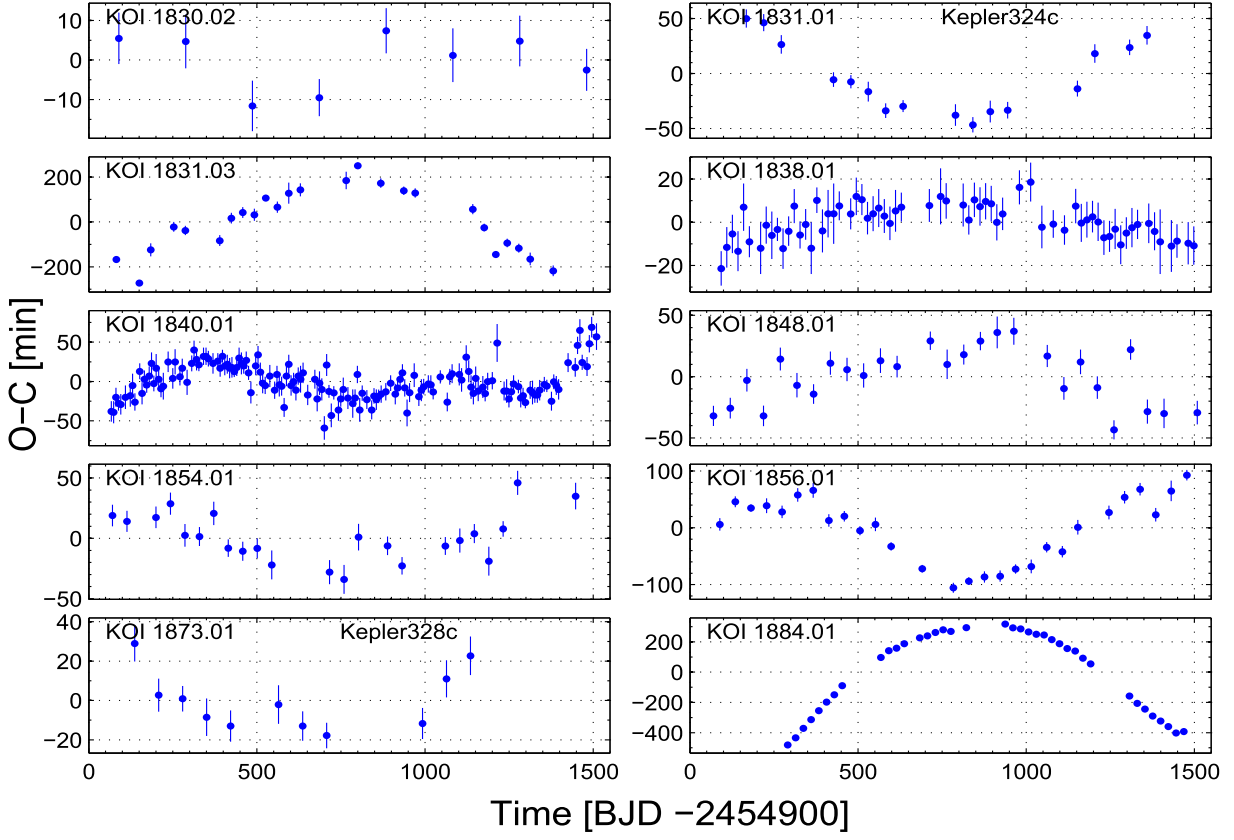


Figure 22. KOIs with significant long-term TTVs.

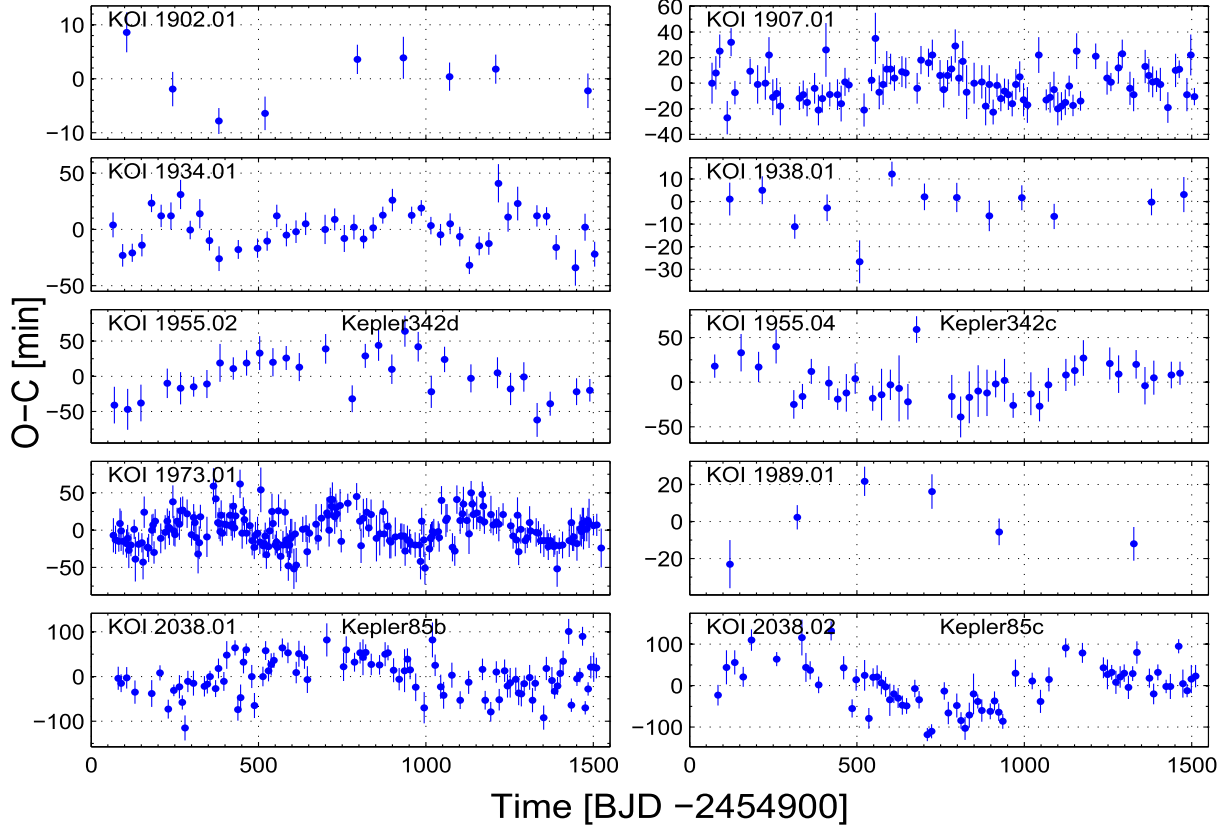


Figure 23. KOIs with significant long-term TTVs.

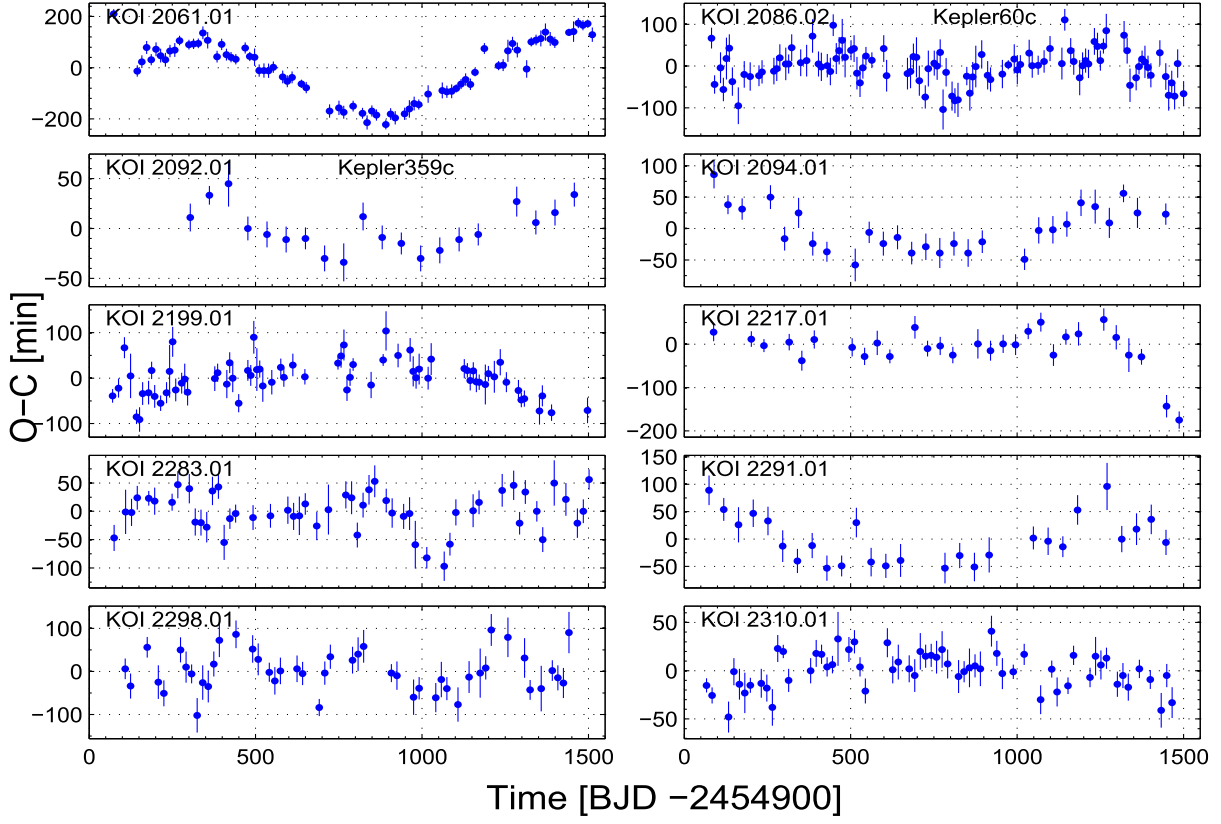


Figure 24. KOIs with significant long-term TTVs.

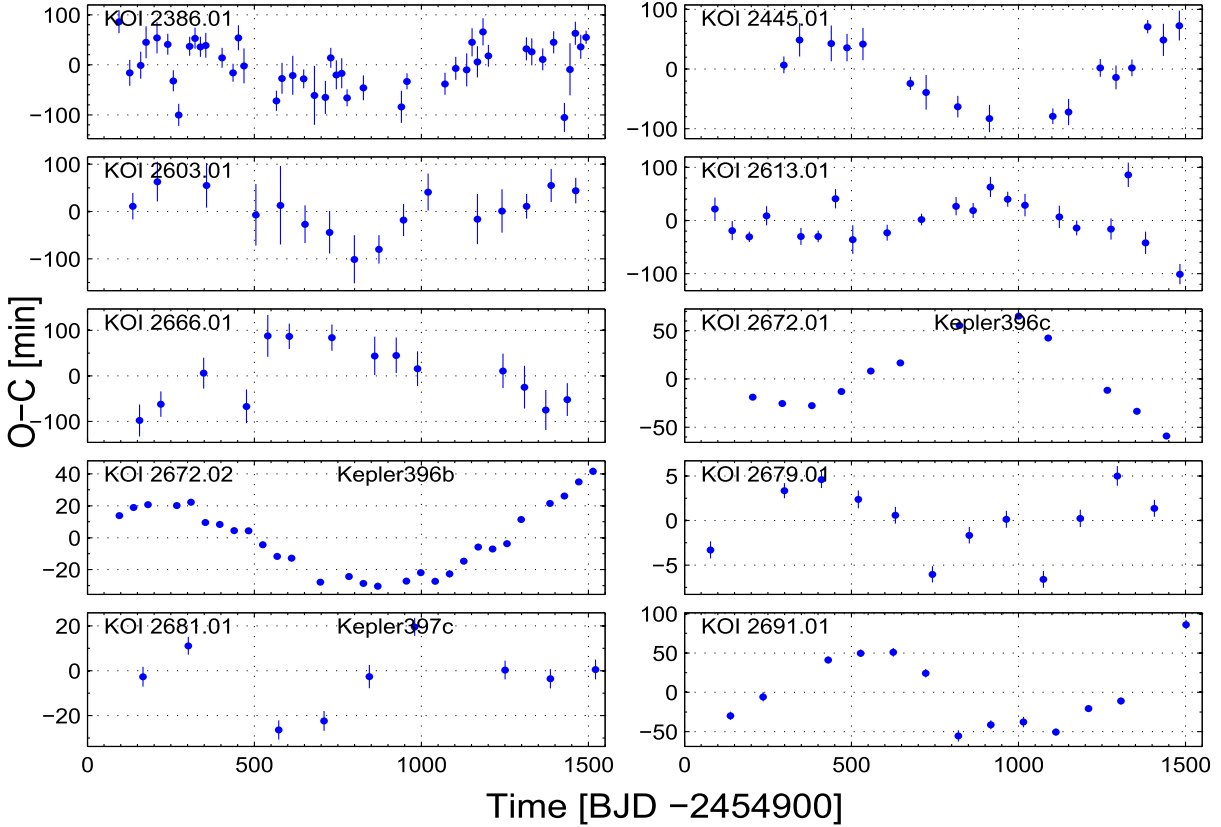


Figure 25. KOIs with significant long-term TTVs.

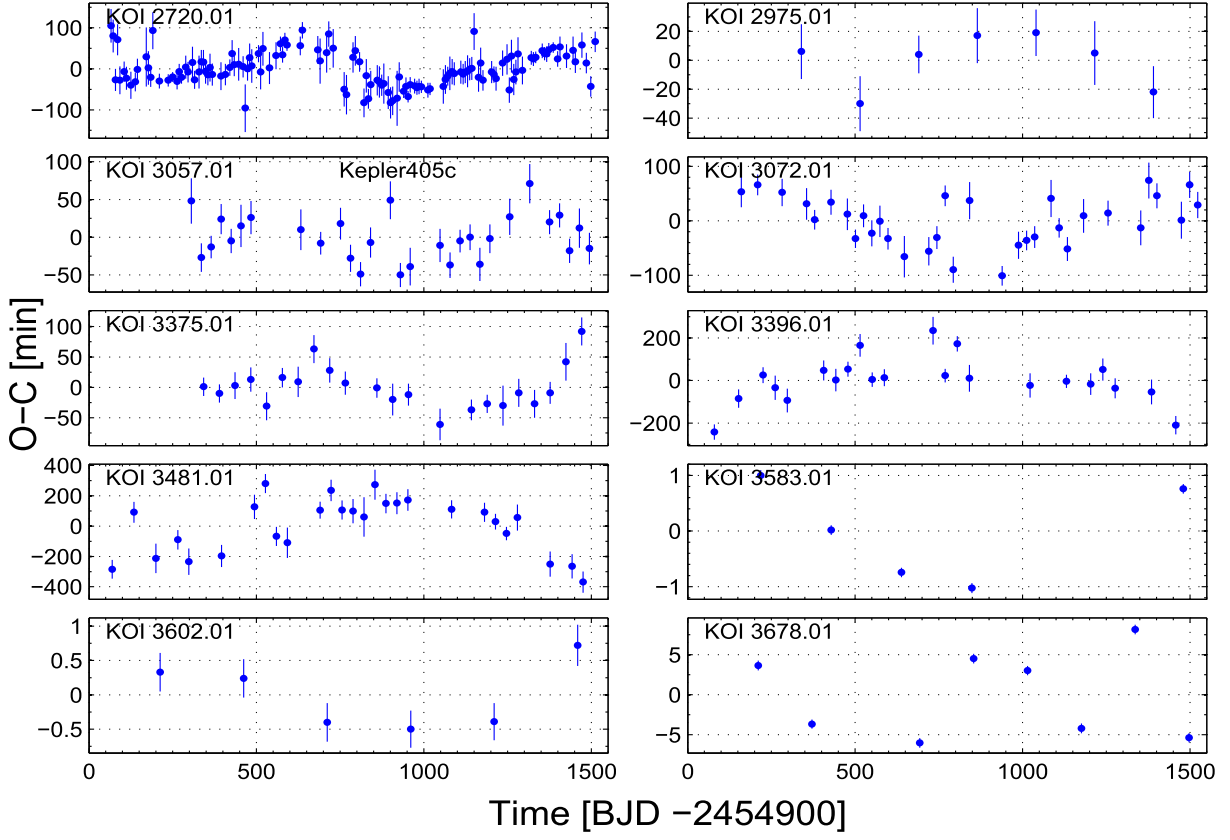


Figure 26. KOIs with significant long-term TTVs.

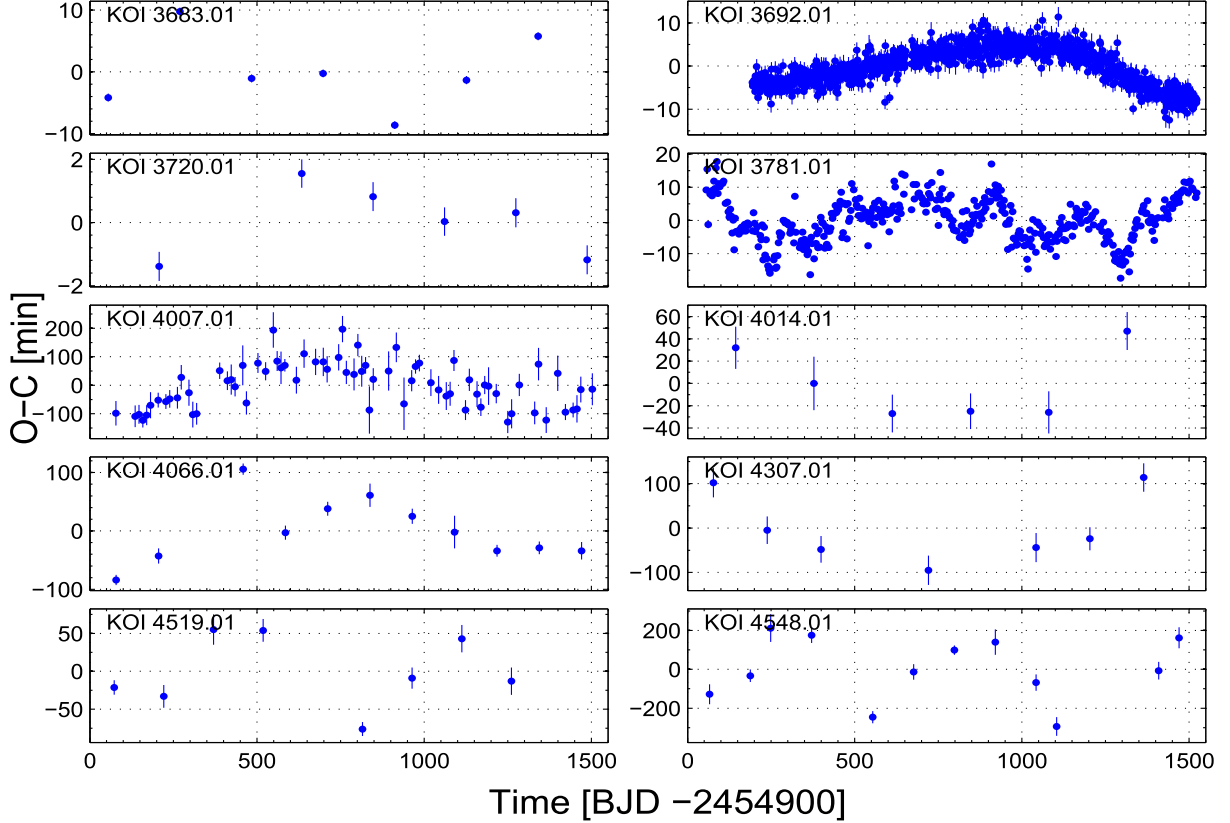


Figure 27. KOIs with significant long-term TTVs.

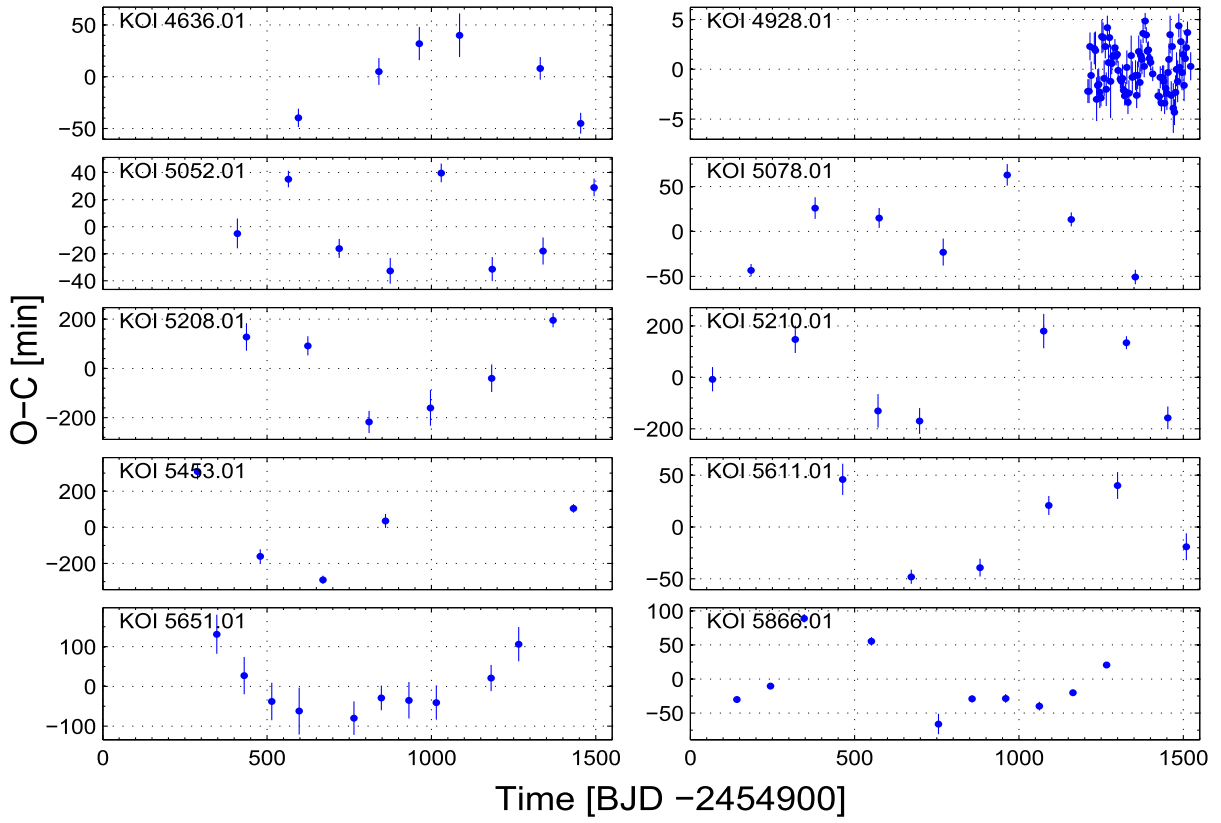


Figure 28. KOIs with significant long-term TTVs.

with the durations and depths of their transits, derived from the folded light curve. The transit duration and depth are quoted in hours and ppm, respectively. For each KOI we also list the SNR of the transit (see above), and the scatter ratio, defined as the ratio between the data scatter inside the transit, relative to the adopted model, and the scatter of the data outside the transit. The two scatters are derived for the folded light curves. Table 3 lists our derived O-Cs, relative to our modified ephemerides, for 295,187 transits of 2599 KOIs. Of those, duration and depth changes, in units of the transit model duration and depth, are given for 69,914 transits of 779 KOIs with $\text{SNR} > 10$, and a transit duration longer than 1.5 hr.

3. IDENTIFYING KOIS WITH SIGNIFICANT LONG-TERM TTVs

As the main focus of this study is the TTVs of the KOIs, the next sections concentrate on the analysis of the derived O-Cs, leaving the analysis of the duration and depth variations for another study. In order to identify KOIs with significant long-term TTVs, we computed a few statistics, listed in Table 4, of the O-C series for 2339 KOIs with more than six timing measurements:

1. The ratio between the median error, $\bar{\sigma}_{\text{TT}}$, and the scatter of the O-Cs, $s_{\text{O-C}}$, (see discussion above and Figure 1). The modified ratio of these two figures, $s_{\text{O-C}}/(1.48\bar{\sigma}_{\text{TT}})$, squared and multiplied by the number of measurements (see Table 3), gave us a modified χ^2 of the O-C series of each KOI. We used this figure to calculate a χ^2 p -value against the no-variation assumption, listed in the table. Very low p -value due to high values of $s_{\text{O-C}}$ relative to $\bar{\sigma}_{\text{TT}}$ might indicate a significant TTV, in particular

because the MAD statistic was less sensitive to outliers than the rms of the O-Cs.

2. A modified power spectrum (PS) periodogram of the O-Cs, presenting for each frequency the energy contained in its fundamental and first harmonic. We identified the highest peak in the periodogram and assigned a p -value to the associated periodicity in the data. This was done by calculating 10^4 modified PS periodograms for different random permutations of the same O-Cs, and counting the number of permutations that had a PS peak higher than the peak of the real data. Table 4 quotes the estimated period and its p -value.
3. An “alarm” \mathcal{A} score of the series, following the statistic of Tamuz et al. (2006), which is sensitive to the correlation between adjacent O-Cs. The value of \mathcal{A} is sensitive to the number of consecutive O-Cs with the same sign, without assuming any functional shape of the modulation (see Tamuz et al. 2006, for a detailed discussion). We assigned a false-alarm probability to the occurrence of the obtained score by calculating alarm scores for 10^4 different random permutations of the same O-C series, and counting the number of permutations that had an alarm higher than the peak of the real data. Table 4 quotes the alarm score and its p -value.
4. A long-term polynomial fit to the O-C series. A significant polynomial fit usually indicates a long-term modulation with a timescale longer than the data span. We searched for a fit with a polynomial with a degree lower than four, chose the best polynomial and tested its significance with an F -test. Table 4 quotes the best polynomial fit and its p -value.

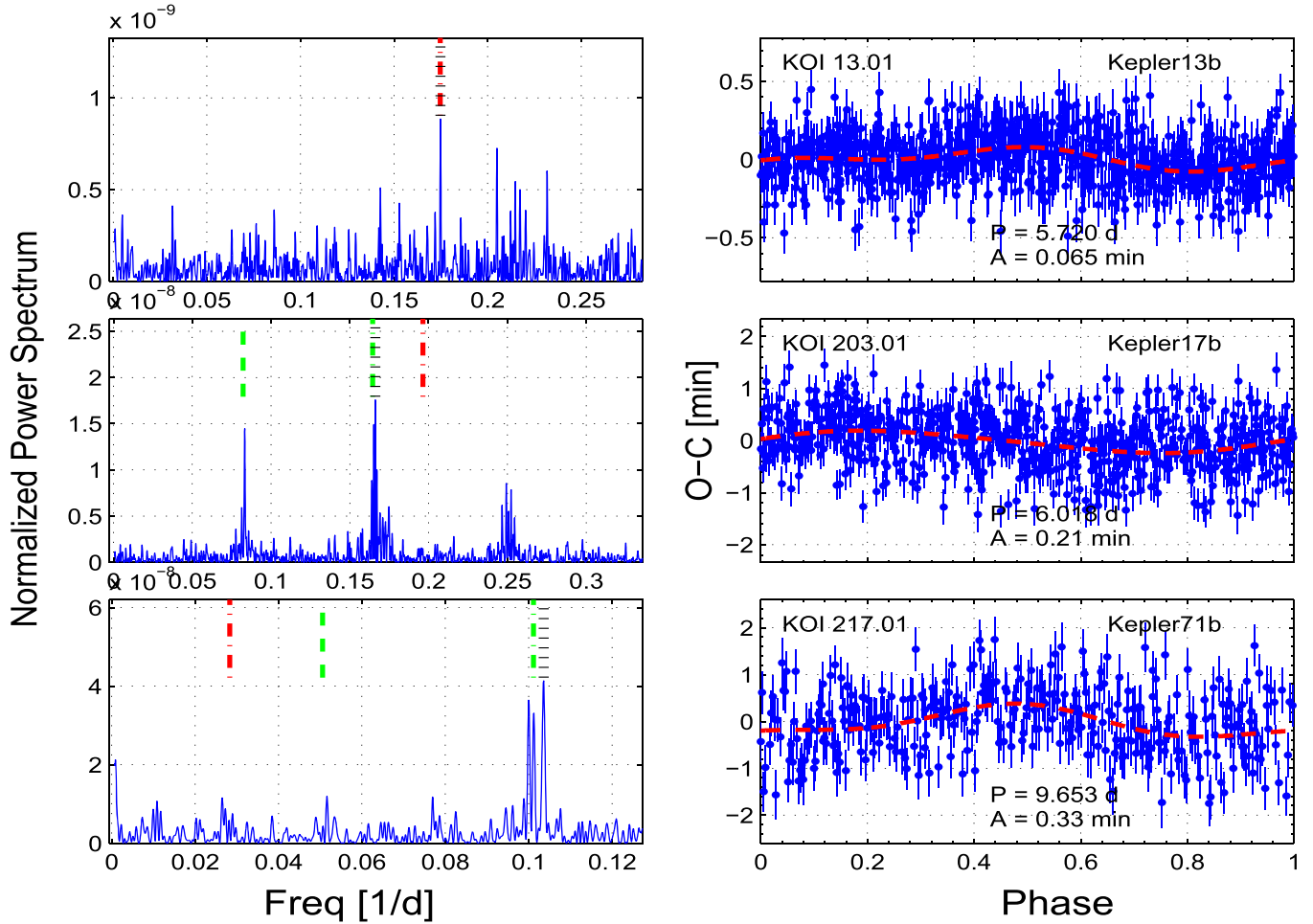


Figure 29. KOIs with short-period TTVs. For each KOI, the plot shows the power spectrum periodogram and the phase-folded O-Cs with the period corresponding to the highest peak (marked by a dotted black line). To emphasize the modulation, we slightly reduced the y-range of the plots of the folded light curves. The dashed green line represents the stellar activity frequency or one of its aliases, if present in the stellar light curve, and the dashed-dotted red line represents the frequency induced by the sampling. The phase-folded light-curve panels include a two-harmonic fit. Period and amplitude are listed in each of the right panels.

4. KOIS WITH LONG-TERM SIGNIFICANT TTVs

Each KOI with any of the aforementioned statistics yielding a p -value lower than 10^{-4} and a period longer than 100 days was identified as having a significant long-term TTV, provided the variation seemed real and not caused by some artifact. Table 5 lists 260 KOIs with long-term significant timing variation and summarizes their variability features, while Figures 3–28 display their TTVs. Of those, 73 KOIs did not pass the significance thresholds, but nevertheless had a relatively high significance and seemed to have a real long-term timing variation, and therefore were also included in the table.

Table 5 lists the KOI number, the orbital period of the transiting planet, and the adopted model, either a Cosine function, “Cos,” or a polynomial “Pol.” For a cosine fit, we list the TTV period and its error, and the amplitude and its error. For the cases with parabolic fits, we list an estimated figure for the amplitude of the variability, based on half the difference between the maximum and minimum values of the parabola at the times of the TTVs. For both types of fitting, we list the scatter of the residuals relative to the adopted fit (which is not plotted). We also list the number of TTV measurements, the multiplicity of the system and references to previous studies, when available.

To derive the TTV periods and amplitudes and their errors we fitted the TTVs with a periodic cosine function superimposed on a linear trend. This was performed by Markov chain Monte Carlo runs, each of which used an ensemble of MCMC samplers (Goodman & Weare 2010; Foreman-Mackey et al. 2013). We summarize the marginal posterior distribution for each period by reporting its median value, along with an uncertainty based on a 68.26% interval ranging from the 15.87th to the 84.13th percentile. Out of 260 KOIs, 199 showed clear significant periodicity, with periods ranging from 100 to over 2000 days, and amplitudes of 1–1470 minutes.

In six special cases—KOI-142.01, -157.03, -417.01, -474.03, -984.01, and -2283.01, we fitted the TTVs with a straight line and *two* different cosine functions, both identified by the MCMC runs. In these cases, Table 5 lists the two periods, and the scatter of the residuals after the removal of the linear trend and the first periodicity, and also after the removal of the linear trend and the two modulations. The secondary periodicity is very clear only in two cases, KOI-142 and -984, as can be seen by comparing the residuals after removing the first and both periodic modulations. Nevertheless, we suggest that the second modulations in the other four cases are also real, especially because our MCMC samplers clearly showed two periodicities.

Table 6
Corrected Periods for KOIs with Periodic Fits

KOI	Period (days)								
12.01	17.8552221 ±0.0000001	166.01	12.4934161 ±0.0000009	303.01	60.9284885 ±0.0000019	500.02	9.5216221 ±0.0000013	775.02	7.8774240 ±0.0000014
42.01	17.8336258 ±0.0000005	168.01	10.7424696 ±0.0000019	308.01	35.5970409 ±0.0000011	520.01	12.7593931 ±0.0000017	784.01	19.2716570 ±0.0000023
84.01	9.2869706 ±0.0000003	168.03	7.1069636 ±0.0000095	314.01	13.781063 ±0.000001	520.03	25.7526459 ±0.0000029	806.01	143.2110706 ±0.0000013
89.01	84.6880617 ±0.0000025	226.01	8.3086708 ±0.0000014	314.02	23.0891043 ±0.0000012	524.01	4.5923909 ±0.0000009	806.02	60.3251041 ±0.0000004
89.02	207.593886 ±0.000016	227.01	17.6746878 ±0.0000062	316.02	157.0645349 ±0.0000078	528.02	96.6783978 ±0.0000052	806.03	29.3235334 ±0.0000029
94.03	54.3199490 ±0.0000008	244.01	12.7203734 ±0.0000002	318.01	38.5844249 ±0.0000007	536.01	81.1694724 ±0.0000049	811.01	20.5058590 ±0.0000015
103.01	14.9109944 ±0.0000007	244.02	6.2385347 ±0.0000003	319.01	46.1511883 ±0.0000006	592.01	39.7530231 ±0.0000042	824.01	15.3756898 ±0.0000006
119.02	190.3211508 ±0.0000027	248.01	7.203863 ±0.000001	345.01	29.8847928 ±0.0000011	598.01	8.3078329 ±0.0000014	829.01	18.6493247 ±0.0000027
137.01	7.6415622 ±0.0000002	248.02	10.9127010 ±0.0000018	370.01	42.8810853 ±0.0000051	620.01	45.1553694 ±0.0000005	829.03	38.5578567 ±0.0000038
137.02	14.8589256 ±0.0000002	250.01	12.2829854 ±0.0000007	372.01	125.6282058 ±0.0000002	620.03	85.3167482 ±0.0000035	834.01	23.6536679 ±0.0000007
139.01	224.834627 ±0.000023	250.02	17.2512300 ±0.0000012	374.01	172.6966450 ±0.0000079	622.01	155.0418161 ±0.0000022	841.01	15.3353712 ±0.0000011
142.01	10.9524820 ±0.0000004	262.01	7.8128264 ±0.0000021	377.01	19.2451976 ±0.0000003	652.01	16.0806593 ±0.0000003	841.02	31.330235 ±0.0000001
152.01	52.0907866 ±0.0000008	262.02	9.3766448 ±0.0000015	377.02	38.9569197 ±0.0000005	672.02	41.7493670 ±0.0000019	868.01	235.996945 ±0.000001
152.02	27.4023653 ±0.0000022	271.02	29.3933073 ±0.0000017	417.01	19.1931004 ±0.0000003	676.01	7.9725076 ±0.0000002	869.02	36.2755108 ±0.0000041
152.03	13.4845592 ±0.0000016	274.01	15.0894194 ±0.0000068	456.01	13.6994490 ±0.0000011	700.01	30.8643155 ±0.0000017	870.01	5.912275 ±0.000001
152.04	81.0643230 ±0.0000073	274.02	22.8038448 ±0.0000084	457.02	7.064259 ±0.0000001	709.01	21.3851880 ±0.0000023	870.02	8.9858347 ±0.0000018
157.01	13.0249115 ±0.0000014	277.01	16.232080 ±0.0000001	464.01	58.3621043 ±0.0000005	730.01	14.7869296 ±0.0000095	872.01	33.6013060 ±0.0000005
157.03	31.9954254 ±0.0000009	277.02	13.848692 ±0.0000006	473.01	12.7062111 ±0.0000016	730.03	19.725722 ±0.0000018	877.02	12.0399070 ±0.0000014
157.04	46.6857474 ±0.0000036	282.01	27.5086337 ±0.0000007	474.03	94.9036924 ±0.0000053	759.01	32.6285963 ±0.0000021	880.01	26.4444855 ±0.0000023
165.01	13.2217598 ±0.0000009	289.01	26.6294667 ±0.0000018	500.01	7.0535152 ±0.0000013	760.01	4.9593200 ±0.0000001	880.02	51.5381149 ±0.0000015
884.02	20.4857821 ±0.0000009	1236.03	54.411731 ±0.0000009	1581.01	29.5420643 ±0.0000057	1934.01	28.7826087 ±0.0000025	2691.01	97.451375 ±0.0000011
886.01	8.0107718 ±0.0000016	1241.02	10.501201 ±0.0000012	1581.02	144.5561670 ±0.0000094	1938.01	96.9153379 ±0.0000033	2720.01	6.5714474 ±0.0000036
886.02	12.0714725 ±0.0000036	1270.02	11.6092377 ±0.0000025	1582.01	186.439063 ±0.000013	1955.04	26.2349240 ±0.0000048	2975.01	175.325064 ±0.000012
918.01	39.6431243 ±0.0000002	1335.01	127.8336764 ±0.0000019	1596.02	105.3584564 ±0.0000076	1973.01	3.2901168 ±0.0000018	3057.01	29.7272764 ±0.0000069
928.01	2.4941748 ±0.0000011	1353.01	125.8645722 ±0.0000009	1599.01	20.411707 ±0.000015	2038.01	8.3053195 ±0.0000038	3375.01	47.059342 ±0.000017
935.01	20.8601883 ±0.0000011	1355.01	51.9291711 ±0.0000014	1622.01	69.8353470 ±0.0000052	2038.02	12.5136311 ±0.0000053	3678.01	160.8845334 ±0.0000004
935.02	42.634082 ±0.0000002	1426.01	38.8684211 ±0.0000025	1628.01	19.7473250 ±0.0000015	2061.01	14.0973940 ±0.0000057	3683.01	214.3122658 ±0.0000018
952.01	5.9012915 ±0.0000014	1426.03	150.0253424 ±0.0000047	1675.01	14.6240689 ±0.0000026	2086.02	8.9189703 ±0.0000048	3781.01	2.8824930 ±0.0000001
984.01	4.289903 ±0.0000022	1429.01	205.9082298 ±0.0000054	1685.01	70.4678845 ±0.0000042	2092.01	57.6898797 ±0.0000087	4066.01	126.563355 ±0.0000016
1061.01	41.809240 ±0.0000017	1472.01	85.3511277 ±0.0000019	1781.03	58.0206109 ±0.0000027	2094.01	42.42631 ±0.00001	4519.01	148.5614006 ±0.0000068
1081.01	9.9564367 ±0.0000026	1474.01	69.7281819 ±0.0000004	1783.01	134.4792915 ±0.0000029	2283.01	17.4022012 ±0.0000052	4548.01	61.076502 ±0.0000022
1086.01	27.6651502 ±0.0000026	1478.01	76.1361284 ±0.0000004	1790.01	130.3569507 ±0.0000029	2298.01	16.6673833 ±0.0000052	4636.01	122.730715

Table 6
(Continued)

KOI	Period (days)								
	± 0.0000065		± 0.0000007		± 0.0000023		± 0.0000078		± 0.000016
1102.01	12.3334799	1503.01	150.2414573	1792.01	88.4066416	2386.01	16.2709167	4928.01	3.2903038
	± 0.0000054		± 0.0000035		± 0.0000011		± 0.0000066		± 0.0000011
1102.02	8.1451227	1529.01	17.9770449	1802.01	5.2486684	2445.01	47.369390	5052.01	155.0469304
	± 0.0000039		± 0.0000069		± 0.0000006		± 0.000012		± 0.0000053
1145.01	30.613636	1546.01	0.917568219	1830.02	198.7110197	2603.01	73.710375	5078.01	194.8995069
	± 0.000013		± 0.00000027		± 0.0000033		± 0.000015		± 0.0000059
1203.03	48.645743	1552.01	77.6343013	1840.01	7.0395672	2613.01	51.571050	5210.01	125.951469
	± 0.000014		± 0.000008		± 0.0000048		± 0.000016		± 0.000036
1209.01	271.0349	1573.01	24.8090474	1854.01	43.0350700	2672.01	88.5080881	5453.01	190.650367
	± 0.0014		± 0.000025		± 0.0000065		± 0.000012		± 0.000016
1215.01	17.324015	1574.01	114.7364914	1856.01	46.300415	2672.02	42.9935242	5611.01	209.215693
	± 0.000004		± 0.000013		± 0.000004		± 0.000014		± 0.000011
1221.02	51.071659	1576.01	10.4157522	1902.01	137.8645887	2679.01	110.7559228	5866.01	102.307114
	± 0.000023		± 0.000011		± 0.0000017		± 0.000006		± 0.000019
1236.01	35.7352604	1576.02	13.0842385	1907.01	11.3500915	2681.01	135.4995035		
	± 0.0000043		± 0.000016		± 0.000019		± 0.000024		

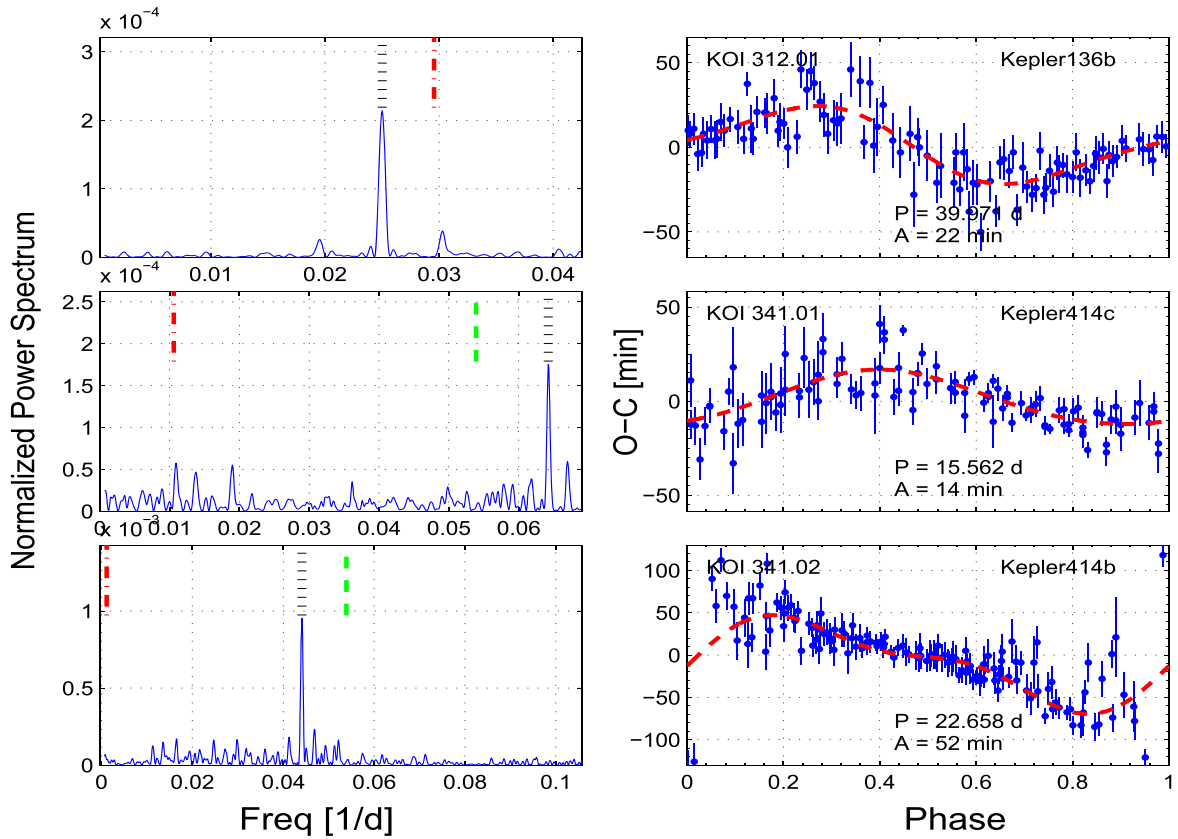


Figure 30. The KOIs with short-period TTVs. For each KOI, the power spectrum periodogram and the phase-folded O-Cs are plotted (see Figure 29 for details).

For 61 KOIs, the cosine function fit was poor, and we therefore fitted instead a simple parabola to the data. This probably meant that the timescale of the modulation was longer than the time span of the data.

The orbital periods listed in Table 2 for the 2599 KOIs were corrected by the slope of the linear fit to the TTVs. This approximation was good when there was no significant long-

term TTV modulation. However, in the presence of a strong TTV periodic modulation, the linear fit by itself might not be good enough, and therefore might yield an inaccurate correction to the orbital period. Therefore, for each of the 199 KOIs that showed a periodic modulation, we have corrected the orbital period using the slope of the linear part of the model in Table 5, which included both a linear slope and

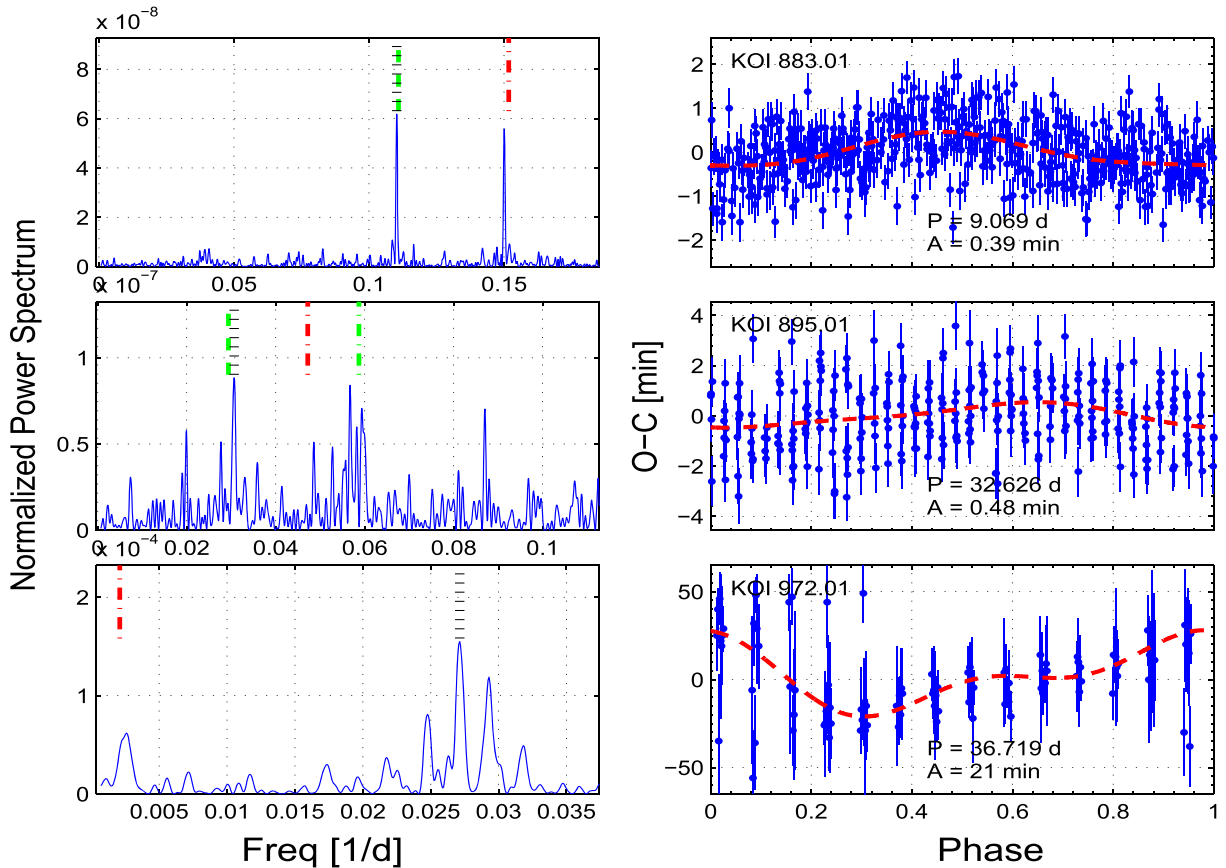


Figure 31. The KOIs with short-period TTVs. For each KOI, the power spectrum periodogram and the phase-folded O-Cs are plotted (see Figure 29 for details).

a cosine modulation. Using the error of the linear slope from the MCMC model might underestimate the uncertainty of the derived orbital period. Instead, we used the difference between the orbital periods obtained by both methods (linear and linear + cosine models) as an error estimate. The new orbital periods and their estimated uncertainties are given in Table 6.

5. KOIS WITH SHORT-PERIOD TTVs

Following the approach of Mazeh et al. (2013), we identified 10 systems with highly significant short-period TTV modulations, in the range of 3–80 days. They were found by obtaining a PS peak with p -value lower than 3×10^{-4} . The modulation amplitudes were relatively small, in the range of 0.07–80 minutes, and their detection was possible only due to the periodic nature of the signal and the long time span of the data relative to the periodicity.

For the sake of comparison, we included in this section plots for KOI-13.01 and -972.01 modulations, which were detected by Mazeh et al. (2013), and our analysis showed the same modulation but with a lower significance. Another seven KOIs that were listed in Mazeh et al. (2013) are not shown here, as they now appear to be false positives and not planet candidates. Two additional systems, KOI-895.01 and -1074.01, are shown because they exhibit TTVs induced by spot crossing events (Holczer et al. 2015).

Figures 29–33 show the PS periodograms with their prominent peaks, and the phase-folded O-Cs of the 14 systems. Table 7 lists the periods and amplitudes found.

As pointed out by Szabó et al. (2013) and discussed by Mazeh et al. (2013), not all detected short-period modulations

are due to physical TTVs. An *apparent* TTV periodicity can be induced either by the long-cadence sampling of *Kepler* (the stroboscopic effect), or by an interference with a periodic stellar activity. To find the frequency of the presumed sampling-induced periodicity, we used for each KOI its P_{orb} from Table 2, and the pertinent P_{samp} . This was about 29.424 minutes for the long cadence, the exact value taken to be the median of the differences of the observed timings of that KOI. We searched for a stellar spot periodicity using the auto-correlation technique (e.g., McQuillan et al. 2013), and, if present, checked whether its frequency and/or one of its harmonics or aliases was equal to the TTV frequency. We mark the pertinent frequencies in Figures 29–33 (see Holczer et al. 2015).

In each of the figures we marked the frequency of the highest peak, the stroboscopic frequency (due to sampling) and the rotational frequency, with its harmonics when relevant. For five systems, KOI-203.01, -217.01, -883.01, -895.01, and -1074.01, the rotational frequency and/or one of its harmonics coincided with the highest periodogram peak (see also Holczer et al. 2015). The periodicity in those cases could be induced by crossing the rotating stellar spots by the transiting planet. Two systems, KOI-883.01 and -13.01, showed a strong stroboscopic effect.

6. TTV PERIODICITIES INDUCED BY AN ADJACENT PLANET NEAR A FIRST-ORDER RESONANCE

As discussed in the introduction, we expect most TTV periodic modulations to be caused by a dynamical interaction with an adjacent additional planet, near first-order resonance

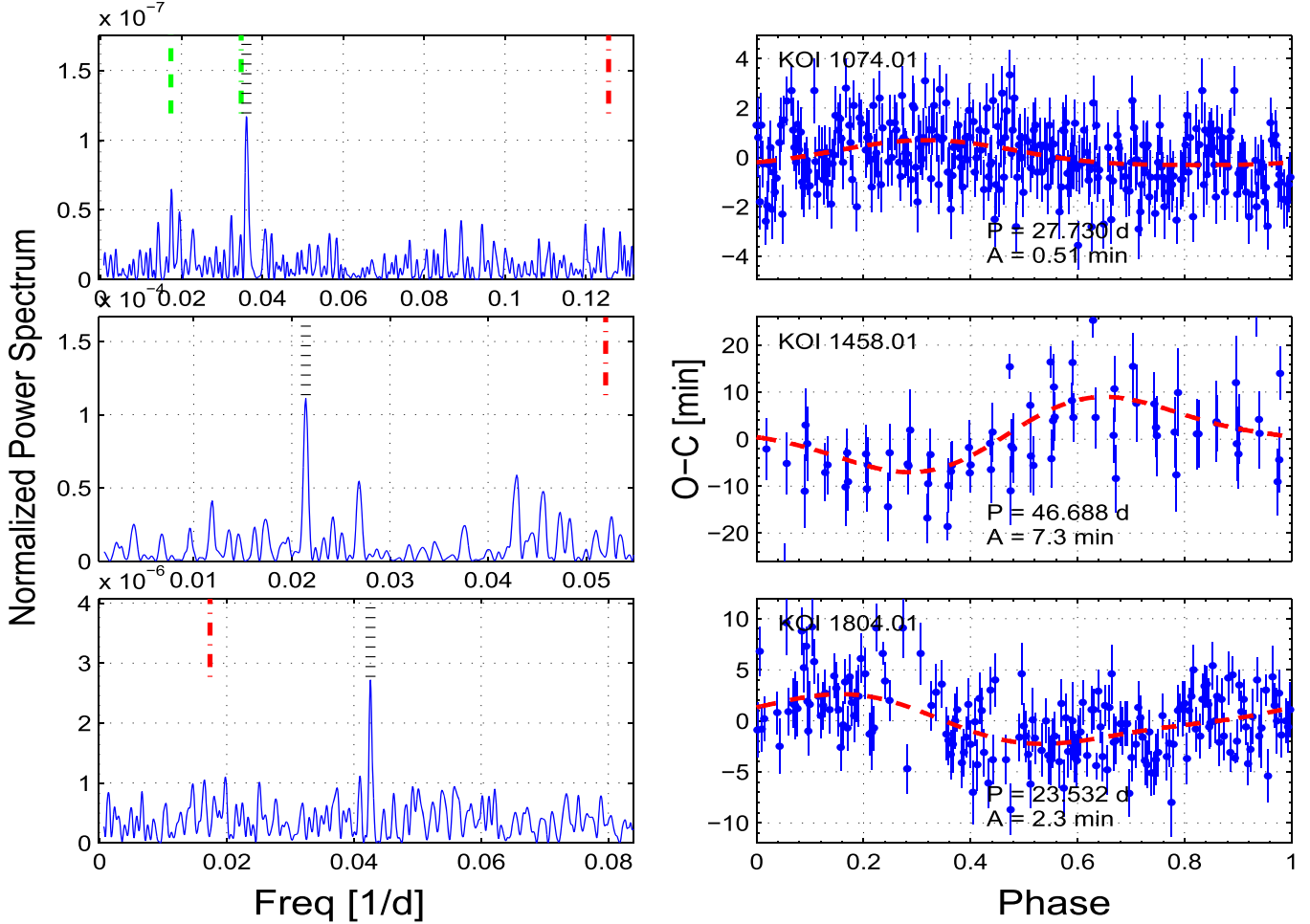


Figure 32. The KOIs with short-period TTVs. For each KOI, the power spectrum periodogram and the phase-folded O-Cs are plotted (see Figure 29 for details).

in particular. For those cases, we have prepared a theoretical infrastructure to calculate the expected TTV period, based on the orbital periods of the two planets (e.g., Lithwick et al. 2012; Hadden & Lithwick 2014). In the case that the adjacent planet is also a transiting one, we should be able to know its orbital period, and therefore to compare the predicted TTV periodicity with the observed one. Thus, we searched the known multiple KOIs systems to see if any additional planet candidate can account for the 199 TTV periodicities of Table 5.

We found 80 pairs of KOIs for which two KOIs resided in the same planetary system and at least one of them showed a clear periodicity as listed in Table 5. Following Xie (2013, 2014), for each of these KOI pairs we checked whether it was close to a first-order resonance by calculating for each of them the normalized distance to the closest first-order resonance, Δ :

$$\Delta \equiv \frac{P_2 j - 1}{P_1 j} - 1, \quad (1)$$

where P_1 and P_2 are the inner and outer orbital periods of the planets of the pair, respectively, and j is the resonance number. We set a cutoff at $\Delta = 0.1$, ignored the pairs with higher values, and found 75 pairs of KOIs that were close to some first-order resonance.

For those pairs we derived the expected super-period P^j , given by

$$P^j \equiv \frac{1}{|j/P_2 - (j-1)/P_1|}, \quad (2)$$

and compared it with the observed TTV periodicities (two if available, otherwise only one observed periodicity) of the pair. We consider this derived super-period as a rough estimate, as the obtained orbital periods of the two transiting planets, P_1 and P_2 , depend on their assumed TTV periodicities. We found 59 pairs, listed in Table 8, for which at least one of the TTV periodicities was consistent with the derived super-period. The table includes the two orbital periods of the pair, the resonance found, the distance to resonance, the calculated super-period, and the observed TTV periodicities with their uncertainties.

Out of the 59 systems, we have found 26 pairs for which the two observed TTV periodicities agreed with each other and also agreed with the calculated super-period, one pair (KOI-250) for which the two observed TTV periodicities agreed with each other but did not agree with their calculated super-period, and 32 pairs for which only one TTV periodicity agreed with the calculated super-period (the other planet did not show any significant periodicity or its TTV period did not agree with the

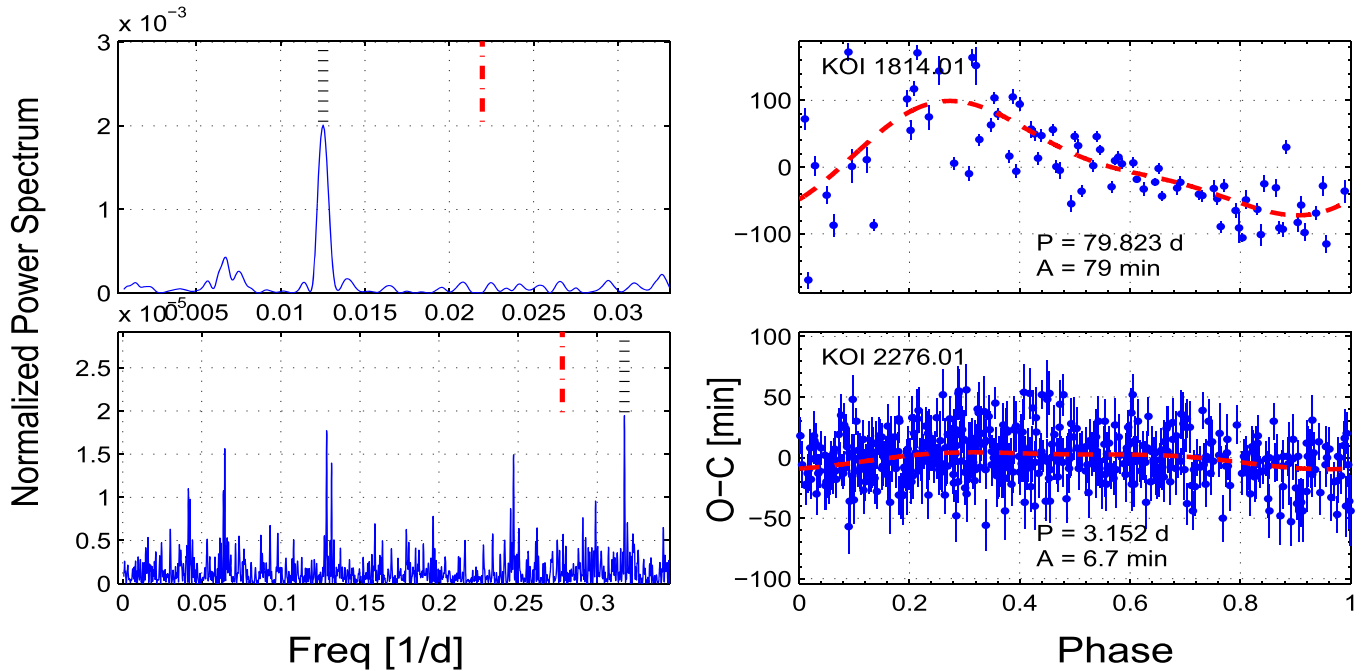


Figure 33. The KOIs with short-period TTVs. For each KOI, the power spectrum periodogram and the phase-folded O-Cs are plotted (see Figure 29 for details).

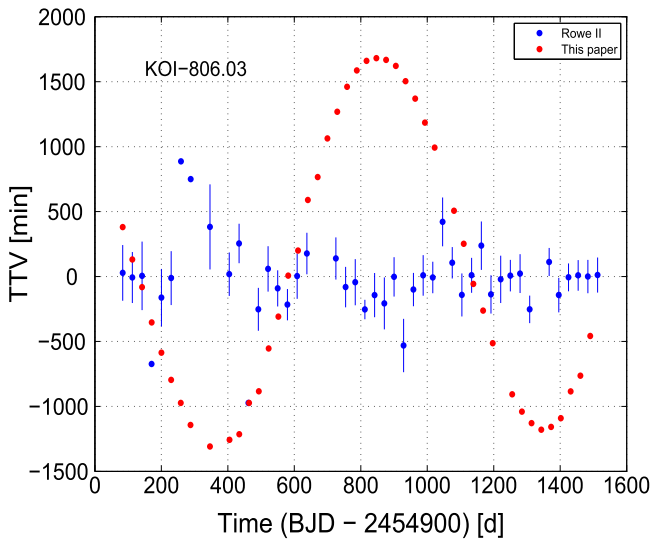


Figure 34. TTV obtained by RoweII (blue) and by this work (red). The error bars of the red points are smaller than the size of their symbols. For each set, the ordinate presents the derived timings, and the abscissa the deviations from the linear ephemeris.

calculated super-period). In one case, KOI-157.03, the derived TTV period was the *second* periodicity found.

To summarize this section, out of the 199 KOIs with periodic TTVs, 84 reside in systems where only one transiting planet is evident. Another 39 KOIs are found in multi-planet systems without an obvious adjacent planet that can explain the detected TTV periodicity. Another 23 KOIs are in multi-planet systems, for which the period of one adjacent planet yields a super-period that is consistent with the observed TTV periodicity. Finally, 53 KOIs show a TTV periodicity that is anti-correlated with TTV modulation of another adjacent planet in the system.

7. COMPARISON WITH THE RECENT CATALOGS

Before concluding, we compare our results with the published KOI catalog by Rowe et al. (2015, RoweI), which also contains the O-C measurements for 5751 KOIs, and with Rowe & Thompson (2015, RoweII) catalog,¹¹ which presents timing measurements for 258 KOIs that they identified as having significant TTV signals. (The criteria used were not given.)

A total of 2290 KOIs were analyzed by this paper and by either RoweI or RoweII. The reason 2014 is that RoweI and II analyzed an extended set of KOIs, including the new batch of identified planet candidates, while we considered the older list of KOIs released in 2013 November. Furthermore, we excluded from the list a set of KOIs that we found to be EBs. Therefore the intersection of the two studies is only 2290 KOIs. In those KOIs, RoweI obtained 275,551 transit timings, while we had a total of 287,428 measurements, and 208,650 timings that were not rejected as outliers. The TTV error estimates were very similar in both works.

We now compare the results of RoweII with the KOIs we found to have significant TTVs (Tables 5 and 7). Out of the 258 KOIs RoweII found with significant TTVs, we have analyzed only 208, out of which 124 KOIs appeared in Table 5, another 4 KOIs appeared in Table 7, and 80 KOIs that we did not identify as variables. On the other hand, we identified 137 KOIs as having significant variability (127/10 in Tables 5/7), which were analyzed by RoweI and were not marked as variables by RoweII. The three sets of timing series derived by the two analyses were carefully compared.

1. 80 KOIs labeled significant by RoweII only—we checked these systems and found most of them not to be significantly variable, both by eye and by our threshold statistics. Only two KOIs (KOI-94.02 and -209.02) actually did (barely) pass our statistic threshold, but we

¹¹ http://exoplanetarchive.ipac.caltech.edu/docs/Kepler_KOI_docs.html

Table 7
KOIs with Significant Short-period TTVs

KOI	Period ^a (days)	Period ^b (days)	σ_p^c (days)	Amp ^d (minutes)	σ_A^e (minutes)	Res ^f (minutes)	N ^g	Multiplicity ^h	References
i13.01	1.76	5.7205	0.0082	0.065	0.0075	0.15	679	1	(1) Kepler13b
203.01	1.49	6.0177	0.009	0.212	0.029	0.51	670	1	(2),(3),(4) Kepler17b
217.01	3.91	9.653	0.033	0.344	0.053	0.67	328	1	(5) Kepler71b
312.01	11.58	39.97	0.32	21.7	1.5	9.6	104	2	(6) Kepler136b
341.01	7.17	15.562	0.06	14.5	1.4	8.5	110	2	(7) Kepler414c
341.02	4.70	22.66	0.1	51.7	2.2	13	142	2	(7) Kepler414b
883.01	2.69	9.069	0.029	0.388	0.041	0.62	468	1	
j895.01	4.41	32.63	0.6	0.48	0.11	1.4	293	1	
i972.01	13.12	36.72	0.34	20.7	1.7	10	99	2	
j1074.01	3.77	27.73	0.38	0.51	0.11	1.2	287	1	
1458.01	8.98	46.69	0.65	7.3	1.3	5.7	78	1	
1804.01	5.91	23.53	0.17	2.27	0.33	2.9	182	1	
1814.01	14.80	79.8	1.9	79.4	7.3	35	77	1	
2276.01	1.44	3.1518	0.003	6.7	1.3	17	459	1	

Notes.^a Orbital Period.^b Best-fit period of the O-C data.^c Period uncertainty.^d The amplitude of the cosine model.^e Amplitude uncertainty.^f Residual scatter (1.483 times their MAD).^g Number of TT measurements.^h Number of planets in the system.ⁱ Added for comparison with Mazeh et al. (2013).^j Added due to spot-crossing related TTVs. (Holczer et al. 2015).

References. (1) Shporer et al. (2011), (2) Desert et al. (2011), (3) Szabó et al. (2013), (4) Bonomo et al. (2012), (5) Howell et al. (2010), (6) Rowe et al. (2014), (7) Hadden & Lithwick (2014).

had removed them from the list, as the data did not seem significant enough.

- 127 KOIs labeled significant by this work only—to check our analysis, we used RoweI timings and still found them to be significantly variable. Just to name a few: KOI-474.03, -841.01, -841.02, -1081.01, -1270.02, -1529.01, -1599.01, and -2061.01 (see Figures 9, 14, 16, 17, 19, 20 and 24).
- 124 KOIs labeled significant by RoweII and by this work—in almost all cases the TTVs were comparable. Only KOI-806.03 displayed timing measurements that were significantly different in the two works. The two sets of derived TTVs are presented in Figure 34 (see also Sanchis-Ojeda et al. 2012). RoweI and RoweII probably missed the actual timings of this KOI because of the large TTVs.

The difference between the works may have resulted from the fact that this work was focused on the TTV variability, while both RoweI and RoweII were studying the general set of KOIs, with the goal of presenting a complete set of planet candidates with analyzed transits.

8. SUMMARY

We presented here a new transit timing catalog of 2599 *Kepler* KOIs, using the PDC-MAP long-cadence light curves that cover the full seventeen quarters of the mission. The catalog included 69,914 transits of 779 KOIs with high enough S/N, for which we derived the best fitting timing, duration and depth for each transit, given the KOI’s best transit template. For additional 225,273 transits of 1820 KOIs with lower S/N, we

derived only the transit timing, keeping the duration and depth fixed for each KOI.

The catalog is available at ftp://wise-ftp.tau.ac.il/pub/tautv/TTV/ver_112, where separate tables for the duration and depth variations are accessible too. In the future, we plan updating the catalog to include short-cadence data and better analysis of overlapping transits.

For each KOI we derived various statistics that can be used to indicate significant variations. Including systems found by previous works, we have found 260 KOIs that showed significant long-term TTVs, with periods longer than 100 days. Of those, 199 KOIs displayed well determined TTV periods and amplitudes. Another 61 KOIs have periods too long to be established without a doubt, and therefore only a parabola was fitted to the TTV series.

It is interesting to compare the analysis of Mazeh et al. (2013) with our results, and to see how the longer time span may change our assessment of the nature of the modulation. For example, after correcting for the TTVs, the deduced orbital periods of KOI-564.01, -1145.01, -1573.01, and -1884.01 were significantly changed; the TTVs of KOI-984.01 showed sinusoidal behavior in the previous catalog, and now display a non-sinusoidal shape with a sharp linear rise; the TTVs of KOI-1599.01 and -1426.01 showed only parabolic behavior in Mazeh et al. (2013), while now allowing for a sinusoidal fit.

For most of the KOIs, we need more data before the TTV period can be robustly determined. However, as the *Kepler* mission in its original mode of operation has been terminated, we do not expect any additional *Kepler* TTVs. The next space missions that will observe the *Kepler* field in a search for transiting planets (e.g., TESS, PLATO), or dedicated ground-

Table 8
KOI Multies

KOI (Inner)	KOI (Outer)	P_1^{a} (Inner) (days)	P_2^{b} (Outer) (days)	Δ^{c}	$j:j-1^{\text{d}}$	$P_{\text{TTV},1}^{\text{e}}$ (Inner) (days)	$\sigma_{P_1}^{\text{f}}$ (days)	$P_{\text{TTV},2}^{\text{g}}$ (Outer) (days)	$\sigma_{P_2}^{\text{h}}$ (days)	P^i (days)	References
137.01	137.02	7.6416	14.8589	0.0278	2:1	269	1	268	1	270	(1),(19),(20) Kepler18
152.02	152.01	27.4024	52.0908	0.0495	2:1	963	47	615	13	530	(2), (3), (13), (20) Kepler79
152.01	152.04	52.0908	81.0643	0.0375	3:2	614	14	741	38	720	(3),(13),(20) Kepler79
152.03	152.02	13.4846	27.4024	0.0161	2:1	849	35	963	47	850	(2),(13),(20) Kepler79
157.06	157.01	10.3040	13.0249	0.0112	5:4	229	3	230	(4),(14),(20) Kepler11
157.03	157.04	31.9954	46.6857	0.0272	3:2	183	2	558	12	570	(4),(14),(20) Kepler11
157.02	157.03	22.6872	31.9954	0.0577	4:3	139	2	140	(4),(14),(20) Kepler11
157.02	157.04	22.6872	46.6857	0.0289	2:1	558	11	810	(4),(14),(20) Kepler11
168.03	168.01	7.1070	10.7425	0.0077	3:2	452	12	443	6	470	(5),(19),(20) Kepler23
244.02	244.01	6.2385	12.7204	0.0195	2:1	326	3	329	4	330	(6),(19),(20) Kepler25
248.01	248.02	7.2039	10.9127	0.0099	3:2	368	3	370	4	370	(7),(20) Kepler49
250.01	250.02	12.2830	17.2512	0.0534	4:3	751	13	734	18	81	(6) Kepler26
262.01	262.02	7.8128	9.3766	0.0001	6:5	1060	24	664	11	10000	(7) Kepler50
271.03	271.02	14.4360	29.3933	0.0181	2:1	1086	65	810	(3) Kepler127
274.01	274.02	15.0894	22.8039	0.0075	3:2	954	29	922	22	1000	(2),(20) Kepler128
277.02	277.01	13.8487	16.2321	0.0047	7:6	439	2	449	1	500	(8) Kepler36
314.03	314.01	10.3120	13.7811	0.0023	4:3	1204	89	1500	(3), (9), (20) Kepler138
377.01	377.02	19.2452	38.9568	0.0121	2:1	1351	0	1353	0	1600	(10), (20) Kepler9
500.01	500.02	7.0535	9.5216	0.0124	4:3	190	2	193	1	190	(2),(17) Kepler80
500.04	500.01	4.6453	7.0535	0.0123	3:2	190	2	190	(2),(17) Kepler80
500.04	500.02	4.6453	9.5216	0.0249	2:1	193	1	190	(2),(17) Kepler80
520.01	520.03	12.7594	25.7526	0.0092	2:1	1294	54	1306	70	1400	(3),(20) Kepler176
620.01	620.03	45.1554	85.3168	0.0553	2:1	789	12	1084	67	770	(7),(20) Kepler51
620.03	620.02	85.3168	130.1781	0.0172	3:2	1084	67	2500	(7),(11),(20) Kepler51
730.01	730.03	14.7869	19.7257	0.0005	4:3	1292	79	1690	100	10000	(3) Kepler223
730.02	730.01	9.8479	14.7869	0.0010	3:2	1292	79	5000	(3) Kepler223
730.04	730.01	7.3840	14.7869	0.0013	2:1	1292	79	6000	(3) Kepler223
730.02	730.03	9.8479	19.7257	0.0015	2:1	1690	100	6500	(3) Kepler223
775.02	775.01	7.8774	16.3848	0.0400	2:1	206	1	200	(7),(20) Kepler52
806.03	806.02	29.3235	60.3251	0.0286	2:1	985	1	969	3	1100	(12), (15), (20) Kepler30
829.01	829.03	18.6493	38.5579	0.0338	2:1	554	20	496	15	570	(7),(20) Kepler53
834.01	834.05	23.6537	50.4472	0.0664	2:1	382	7	380	(2) Kepler238
841.01	841.02	15.3354	31.3302	0.0215	2:1	723	11	717	8	730	(6),(20) Kepler27
869.03	869.02	17.4608	36.2755	0.0388	2:1	597	8	470	(3) Kepler245
870.01	870.02	5.9123	8.9858	0.0132	3:2	230	2	230	3	230	(6),(19),(20) Kepler28
877.01	877.02	5.9549	12.0399	0.0109	2:1	535	12	550	(2),(20) Kepler81
880.01	880.02	26.4445	51.5383	0.0255	2:1	969	34	1213	13	1000	(2),(20) Kepler82
886.01	886.02	8.0108	12.0715	0.0046	3:2	850	5	852	6	870	(7),(20) Kepler54
935.01	935.02	20.8602	42.6341	0.0219	2:1	940	13	1162	42	970	(12), (20) Kepler31
935.02	935.03	42.6341	87.6476	0.0279	2:1	1162	42	1600	(12), (20) Kepler31
952.01	952.02	5.9013	8.7521	0.0113	3:2	267	4	260	(12), (19), (20) Kepler32
1102.02	1102.01	8.1451	12.3335	0.0095	3:2	440	8	413	7	430	(5),(19),(20) Kepler24
1203.01	1203.03	31.8838	48.6457	0.0171	3:2	821	38	950	(2),(20) Kepler276
1215.01	1215.02	17.3240	33.0067	0.0474	2:1	348	8	350	(2),(20) Kepler277
1236.01	1236.03	35.7353	54.4117	0.0151	3:2	1194	23	1254	21	1200	(2),(18) Kepler279
1241.02	1241.01	10.5012	21.4057	0.0192	2:1	542	6	560	(7),(20) Kepler56
1270.01	1270.02	5.7293	11.6092	0.0131	2:1	456	5	440	(7),(20) Kepler57
1426.01	1426.02	38.8684	74.9285	0.0361	2:1	1040	20	1000	(3),(16),(20) Kepler297
1426.02	1426.03	74.9287	150.0254	0.0011	2:1	1322	60	60000	(3),(16),(20) Kepler297
1529.02	1529.01	11.8682	17.9770	0.0098	3:2	618	9	610	(7) Kepler59
1576.01	1576.02	10.4158	13.0842	0.0050	5:4	517	24	481	20	530	(2),(20) Kepler307
1599.02	1599.01	13.6141	20.4117	0.0005	3:2	1487	37	15000	
1783.01	1783.02	134.4793	284.0423	0.0561	2:1	1390	140	2500	
1955.04	1955.02	26.2349	39.4572	0.0027	3:2	563	28	5000	(3) Kepler342
2038.01	2038.02	8.3053	12.5136	0.0045	3:2	1091	42	1008	28	930	(2),(18),(20) Kepler85
2038.02	2038.04	12.5136	25.2177	0.0076	2:1	1008	28	1700	(3),(18),(20) Kepler85

Table 8
(Continued)

KOI (Inner)	KOI (Outer)	P_1^{a} (Inner) (days)	P_2^{b} (Outer) (days)	Δ^{c}	$j:j-1^{\text{d}}$	$P_{\text{TTV},1}^{\text{e}}$ (Inner) (days)	$\sigma_{P_1}^{\text{f}}$ (days)	$P_{\text{TTV},2}^{\text{g}}$ (Outer) (days)	$\sigma_{P_2}^{\text{h}}$ (days)	P^j (days)	References
2086.01	2086.02	7.1316	8.9190	0.0005	5:4	715	28	3600	(7) Kepler60
2092.01	2092.03	57.6899	77.0870	0.0022	4:3	1280	130	9000	(3) Kepler359
2672.02	2672.01	42.9935	88.5081	0.0293	2:1	1516	32	1303	11	1500	(2),(18) Kepler396

Notes.^a Orbital period of the inner planet.^b Orbital period of the outer planet.^c Normalized distance to resonance defined as $\Delta \equiv \frac{P_2 j - 1}{P_1 j} - 1$ (Lithwick et al. 2012).^d Resonance type.^e The TTV period of the inner planet (found by modeling the data).^f The TTV period uncertainty of the inner planet.^g The TTV period of the outer planet (found by modeling the data).^h The TTV period uncertainty of the inner planet.ⁱ The TTV super-period inferred from the orbital periods: $P^j \equiv \frac{1}{|j/P_2 - (j-1)/P_1|}$.^j The second strongest TTV period.

References. (1) Cochran et al. (2011), (2) Xie (2014), (3) Rowe et al. (2014), (4) Lissauer et al. (2011a), (5) Ford et al. (2012a), (6) Steffen et al. (2012a), (7) Steffen et al. (2013), (8) Carter et al. (2012), (9) Kipping et al. (2014), (10) Holman et al. (2010), (11) Masuda (2014), (12) Fabrycky et al. (2012), (13) Jontof-Hutter et al. (2014), (14) Lissauer et al. (2013), (15) Sanchis-Ojeda et al. (2012), (16) Diamond-Lowe et al. (2015), (17) Ragozzine & Kepler Team (2012), (18) Yang et al. (2013), (19) Lithwick et al. (2012), (20) Hadden & Lithwick (2014).

based follow-up observations (e.g., Raetz et al. 2014), may be very useful for determining the true nature and TTV periodicity of these systems.

Most of the significant TTVs presented here are probably due to dynamical interaction with another planet(s), either transiting or still unknown. The present catalog includes 121 single KOIs with significant long-term modulations, probably caused by undetected additional planets, and therefore are multi-planet systems. The missing planets can be divided into two classes: (1) small planets that were not detected by the present analysis of *Kepler*'s data, either because the transits were too shallow and/or the transit timings were shifted by the dynamical interaction with the known planet, so that the folding of the light curve could not reveal the shallow; and (2) planets with high enough inclinations, so they do not pass in front of their parent stars.

One could hope that the accumulating details of the observed TTVs could give some hints for the orbital elements of the perturbing unseen planet. However, as discussed already by Holman & Murray (2005) and Agol et al. (2005), the amplitude and periodicity of the TTV modulation depends on various parameters, in particular the mass and the orbital period of the unseen planet, and how close the orbits of the two planets are to some mean motion resonance (e.g., Lithwick et al. 2012). Therefore, it is quite difficult to deduce the parameters of the unseen planet. In selected cases, some stringent constraints can be derived, as was done by Ballard et al. (2011) and Nesvorný et al. (2012, 2013). We hope that our catalog will motivate a similar work on other single-KOI systems, as well as on the multi-planet systems, with significant TTVs.

Ten systems analyzed here showed significant, small amplitude modulations with periods shorter than 100 days. We presented these ten systems together with another two systems, whose modulations were detected by Mazeh et al. (2013) and still showed periodic, but less significant, modulations, and another two KOIs that displayed photometric slope correlated with the TTVs, found by Holczer et al. (2015). Out

of the 13 systems found by Mazeh et al. (2013) with short-period modulation, 7 now appear to be false positives, and the other 6 are presented here.

The short-period modulations might not be due to dynamical interaction with another planet, but could be due to either the long cadence sampling of *Kepler*, or the stellar spots periodic activity. For five systems, the stellar rotational frequency and/or one of its harmonics coincide with the highest peak (see also Holczer et al. 2015) of the derived periodogram. Two systems, KOI-883.01 and -13.01, show a strong stroboscopic effect. The stars with TTVs related to the stellar spot activity are interesting, because the transit timings can shed some light on the stellar spot activity, as was shown very recently by Mazeh et al. (2015, 2015) and Holczer et al. (2015).

Finally, one could expect that the derived TTVs, for the single KOIs in particular, could help in constructing a *statistical* picture of the frequency and architecture of the population of the planetary multiple systems of the *Kepler* KOIs (e.g., Steffen et al. 2010; Ford et al. 2011, 2012b; Lissauer et al. 2011b; Fabrycky et al. 2014). To perform such a statistical analysis one needs to model the dependence of the detectability of long-term TTV coherent modulations on the parameters of the unseen perturbing planet. The present catalog can be used for such a study.

We are indebted to the referee for careful reading of the paper and for many thoughtful and helpful comments and suggestions. The research leading to these results has received funding from the European Research Council under the EU's Seventh Framework Programme (FP7/(2007-2013))/ERC Grant Agreement No. 291352), the ISRAEL SCIENCE FOUNDATION (grant No. 1423/11), and the Israeli Centers of Research Excellence (I-CORE, grant No. 1829/12). E.B.F. was supported in part by NASA Kepler Participating Scientist Program award # NNX14AN76G. All photometric data presented in this paper were obtained from the Mikulsky Archive for Space Telescopes (MAST). STScI is operated by the Association of Universities

for Research in Astronomy, Inc., under NASA contract NAS5-26555. Support for MAST for non-*HST* data is provided by the NASA Office of Space Science via grant NNX09AF08G and by other grants and contracts.

REFERENCES

- Agol, E., & Deck, K. 2015, in American Astronomical Society Meeting Abstracts 225, #105.07
- Agol, E., Steffen, J., Sari, R., & Clarkson, W. 2005, *MNRAS*, 359, 567
- Ballard, S., Fabrycky, D., Fressin, F., et al. 2011, *ApJ*, 743, 200
- Batalha, N. M., Rowe, J. F., Bryson, S. T., et al. 2013, *ApJS*, 204, 24
- Bonomo, A. S., Hébrard, G., Santerne, A., et al. 2012, *A&A*, 538, A96
- Carter, J. A., Agol, E., Chaplin, W. J., et al. 2012, *Sci*, 337, 556
- Claret, A., & Bloemen, S. 2011, *A&A*, 529, A75
- Cochran, W. D., Fabrycky, D. C., Torres, G., et al. 2011, *ApJS*, 197, 7
- Dawson, R. I., Johnson, J. A., Fabrycky, D. C., et al. 2014, *ApJ*, 791, 89
- Deleuil, M., Almenara, J.-M., Santerne, A., et al. 2014, *A&A*, 564, A56
- Desert, J.-M., Charbonneau, D., Demory, B.-O., et al. 2011, *ApJS*, 197, 14
- Diamond-Lowe, H., Stevenson, K. B., Fabrycky, D., et al. 2015, in American Astronomical Society Meeting Abstracts 225, #438.01
- Fabrycky, D. C., Ford, E. B., Steffen, J. H., et al. 2012, *ApJ*, 750, 114
- Fabrycky, D. C., Lissauer, J. J., Ragozzine, D., et al. 2014, *ApJ*, 790, 146
- Ford, E. B., Fabrycky, D. C., Steffen, J. H., et al. 2012a, *ApJ*, 750, 113
- Ford, E. B., Ragozzine, D., Rowe, J. F., et al. 2012b, *ApJ*, 756, 185
- Ford, E. B., Rowe, J. F., Fabrycky, D. C., et al. 2011, *ApJS*, 197, 2
- Foreman-Mackey, D., Conley, A., Meierjungen Farr, W., et al. 2013, emcee: The MCMC Hammer Astrophysics Source Code Library, ascl:1303.002
- Goodman, J., & Weare, J. 2010, *Comm. App. Math. Comp. Sci.*, 5, 65
- Hadden, S., & Lithwick, Y. 2014, *ApJ*, 787, 80
- Holczer, T., Shporer, A., Mazeh, T., et al. 2015, arXiv:1504.04028
- Holman, M. J., Fabrycky, D. C., Ragozzine, D., et al. 2010, *Sci*, 330, 51
- Holman, M. J., & Murray, N. W. 2005, *Sci*, 307, 1288
- Howell, S. B., Rowe, J. F., Sherry, W., et al. 2010, *ApJ*, 725, 1633
- Howell, S. B., Sobeck, C., Haas, M., et al. 2014, *PASP*, 126, 398
- Jontof-Hutter, D., Lissauer, J. J., Rowe, J. F., & Fabrycky, D. C. 2014, *ApJ*, 785, 15
- Kipping, D. M., Nesvorný, D., Buchhave, L. A., et al. 2014, *ApJ*, 784, 28
- Lissauer, J. J., Fabrycky, D. C., Ford, E. B., et al. 2011a, *Natur*, 470, 53
- Lissauer, J. J., Jontof-Hutter, D., Rowe, J. F., et al. 2013, *ApJ*, 770, 131
- Lissauer, J. J., Ragozzine, D., Fabrycky, D. C., et al. 2011b, *ApJS*, 197, 8
- Lithwick, Y., Xie, J., & Wu, Y. 2012, *ApJ*, 761, 122
- Mandel, K., & Agol, E. 2002, *ApJL*, 580, L171
- Marcy, G. W., Isaacson, H., Howard, A. W., et al. 2014, *ApJS*, 210, 20
- Masuda, K. 2014, *ApJ*, 783, 53
- Mazeh, T., Holczer, T., & Shporer, A. 2015, *ApJ*, 800, 142
- Mazeh, T., Nachmani, G., Holczer, T., et al. 2013, *ApJS*, 208, 16
- Mazeh, T., Perets, H. B., McQuillan, A., & Goldstein, E. S. 2015, *ApJ*, 801, 3
- McQuillan, A., Aigrain, S., & Mazeh, T. 2013, *MNRAS*, 432, 1203
- Nesvorný, D., Kipping, D., Terrell, D., et al. 2013, *ApJ*, 777, 3
- Nesvorný, D., Kipping, D., Terrell, D., & Feroz, F. 2014, *ApJ*, 790, 31
- Nesvorný, D., Kipping, D. M., Buchhave, L. A., et al. 2012, *Sci*, 336, 1133
- Ofir, A., Dreizler, S., Zechmeister, M., & Husser, T.-O. 2014, *A&A*, 561, A103
- Raetz, S., Maciejewski, G., Ginski, C., et al. 2014, *MNRAS*, 444, 1351
- Ragozzine, D., & Kepler Team 2012, in AAS/Division for Planetary Sciences Meeting Abstracts 44, #200.04
- Rowe, J. F., Bryson, S. T., Marcy, G. W., et al. 2014, *ApJ*, 784, 45
- Rowe, J. F., Coughlin, J. L., Antoci, V., et al. 2015, *ApJS*, 217, 16
- Rowe, J. F., & Thompson, S. E. 2015, arXiv:1504.00707
- Sanchis-Ojeda, R., Fabrycky, D. C., Winn, J. N., et al. 2012, *Natur*, 487, 449
- Shporer, A., Jenkins, J. M., Rowe, J. F., et al. 2011, *AJ*, 142, 195
- Steffen, J. H., Batalha, N. M., Borucki, W. J., et al. 2010, *ApJ*, 725, 1226
- Steffen, J. H., Fabrycky, D. C., Agol, E., et al. 2013, *MNRAS*, 428, 1077
- Steffen, J. H., Fabrycky, D. C., Ford, E. B., et al. 2012a, *MNRAS*, 421, 2342
- Steffen, J. H., Ford, E. B., Rowe, J. F., et al. 2012b, *ApJ*, 756, 186
- Szabó, R., Szabó, G. M., Dálya, G., et al. 2013, *A&A*, 553, A17
- Tamuz, O., Mazeh, T., & North, P. 2006, *MNRAS*, 367, 1521
- Van Eylen, V., Lund, M. N., Silva Aguirre, V., et al. 2014, *ApJ*, 782, 14
- Wang, J., Xie, J.-W., Barclay, T., & Fischer, D. A. 2014, *ApJ*, 783, 4
- Weiss, L. M., Marcy, G. W., Rowe, J. F., et al. 2013, *ApJ*, 768, 14
- Winn, J. N. 2011, *European Physical Journal Web of Conferences*, 11 5002
- Xie, J.-W. 2013, *ApJS*, 208, 22
- Xie, J.-W. 2014, *ApJS*, 210, 25
- Yang, M., Liu, H.-G., Zhang, H., Yang, J.-Y., & Zhou, J.-L. 2013, *ApJ*, 778, 110